



Loss Modeling of Rollover for Autonomous Vehicles





Loss Modeling of Rollover for Autonomous Vehicles

AUTHORS Petar Jevtic Ph.D. (PI)(Arizona State University)
Yan Chen Ph.D. (Co-PI)(Arizona State University)
Yue Shi Ph.D. (Postdoc)(Arizona State University)

SPONSOR Society of Actuaries' Research Expanding
Boundaries Pool

Caveat and Disclaimer

The opinions expressed and conclusions reached by the authors are their own and do not represent any official position or opinion of the Society of Actuaries or its members. The Society of Actuaries makes no representation or warranty to the accuracy of the information

Copyright © 2019 by the Society of Actuaries. All rights reserved.

CONTENTS

Section 1: Introduction	5
1.1 Main Insight	5
1.2 Mathematical Model.....	5
1.3 Rollover Index (RI)	7
Section 2: Critical Maneuvers and Main Perturbances.....	12
2.1 Critical Maneuvers.....	12
2.2 Main Perturbances	16
Section 3: Mixture Model for Offset Distribution	19
3.1 Dependence of Offset on the Maneuver Type, Road Type and Speed	19
3.2 Formulating a Mixture Model.....	19
3.3 Using CarSim Software to Discover the Component or (sub-) Distributions	20
3.4 Simulation and Experimental Results	21
Section 4: Integration with Google Maps	24
4.1 Route 1: Aggressive Driving Strategy.....	24
4.2 Route 2: Normal Driving Strategy.....	27
Section 5: Simulation and Experimental Validation	30
5.1 The Lab’s Vehicle Parameters	30
5.2 Validation Process	31
Appendix A: QQ Plots	34
Endnotes	37
References.....	38
About The Society of Actuaries	40

Loss Modeling of Rollover for Autonomous Vehicles

Automation in vehicles has been attracting attention from both industrial and academic perspectives for years. For conventional and semi-autonomous vehicles, vehicle safety is shared between human drivers and various kinds of driving assistance systems, e.g. crash warning system, adaptive cruise control, lane-keeping systems. Autonomous vehicles, in contrast, take full responsibility for the safety and stability for itself as well as its passengers and surrounding subjects. As such, an autonomous driving system is a new type of driver, of which the insurance industry has no historical experience. However, at least in the case of rollover risk, compared to a human driver, the new driver might turn to be easier to understand.

Unlike human drivers, the autonomous driving systems generally employ a “sense-plan-act” design. After gathering environmental information via a suite of sensors, software algorithms interpret the data to plan and decide consequent vehicle behaviors, including trajectory towards a destination, speed, and maneuvers. The plan/decision is finally implemented by vehicle control systems and actuators, via steering, throttle and brake control. Despite the reliability issues (e.g. sensor/system failure) of the autonomous driving systems itself, it is important to realize that autonomous vehicles may also suffer from some of the dynamical safety problems to those of conventional vehicles. Here, from a vehicle dynamics point of view, there are three major categories of risks for autonomous vehicles, namely collision, lateral instability, and rollover.

The research shows that nearly one-third of crashes can be prevented with systems such as forward collision and lane-departure warning, blind-spot assist, and automatic braking on board [1]. Also, vehicle stability control, specifically for lateral acceleration and yaw rate regulation has been studied for conventional vehicles, and many practical approaches can and have been explored for autonomous vehicles, e.g. in [2], [3] and [4]. On the other hand, rollover is a type of critical vehicle crash in which a vehicle tips over onto its side or roof. Rollover is more commonly observed for vehicles with a high center of gravity (CG) positions, such as SUVs and trucks. However, rollover risk of autonomous vehicles is underestimated in the academic literature. Currently, very few studies specifically take rollover prevention into account during autonomous driving system design. In addition, vehicle parameter uncertainty (e.g. variation of CG height/position due to distribution of the goods in the cargo) and environmental perturbation (e.g. variation of tire-road friction condition) also worsens the situation. This work, by creating a probabilistic model of rollover, simultaneously aims to address this deficiency of the literature as well as give methodological tools for an insurer to better understand the potential losses incurred by autonomous vehicles in the context of rollover risk.

This report is organized as follows. In Section 1, we introduce the main insight, mathematical model, and rollover index. Section 2 presents the critical maneuvers and main sources of perturbation that can affect them. In Section 3, the mixture modes for the offset distribution are articulated, and Section 4 for two realistic scenarios shows numerical results of rollover probabilities and loss distribution, which integrated with Google maps. Section 5 gives experimental validations of the loss modeling. The Endnote concludes the report.

Section 1: Introduction

The main difference between human drivers and autonomous driving systems is that for latter ones, the specific driving trajectory is planned, and the manifested trajectory can be measured. This main conceptual insight will be used as a basis for a mathematical model for the probability of rollover and, consequently, building a loss model. The onset of rollover is intimately tied to the rollover region, which will be described in this section.

1.1 Main Insight

In autonomous driving, the term ‘trajectory’ has both macro-scale (global trajectory) and micro-scale (local trajectory) meanings. A global trajectory (or so-called ‘route’) can be defined as a geometric path, linking the vehicles’ current place and the final destination, along with an assigned velocity profile defining a desired vehicle speed along the path; a local trajectory mostly refers to a short trajectory, with both path and velocity profile, for a specific maneuver, e.g. cornering, lane change, etc. [5].

The planned trajectory that a human driver will take during driving, at the current level of technology, is inaccessible information that is empirical in human minds. What is observable when it comes to a human driver is the trajectory taken. Autonomous driving systems fundamentally differ when it comes to trajectory planning. With autonomous driving systems, we know the planned trajectory, as we choose it on our own, and, the same as with a human driver, we can observe the trajectory that is taken. Thus, importantly, there is an offset between the planned trajectory and the realized trajectory that can be measured when autonomous driving systems are involved. There are various (random) external conditions (weather, road condition, etc.) and internal conditions (mechanical, electric response times, etc.), which can explain why this offset occurs. Those conditions make an offset to be random in nature.

In this work, the primary focus will be on developing a mathematical framework for understanding a rollover risk of an autonomous driving system. Further research will be needed on mathematical models of human drivers and their integrations in the probabilistic framework to be developed here.

1.2 Mathematical Model

From mathematical perspective, a planned trajectory (P) for an autonomous vehicle is a sequence of planned (p) points in a high dimensional space

$$P = \{(x_i^p, y_i^p, V_i^p, t_i^p)\}_{i=1}^{i=N}$$

Here, with x_i^p and y_i^p we denote latitude and longitude respectively, with t_i^p time index, and with V_i^p a vehicle speed. Now, depending on maneuvers, such as single lane change, double lane change or lane keeping, implicitly, the planned trajectory can consists of

$$P = \{(x_i^p, y_i^p, V_i^p, t_i^p, a_{y_i}^p, r_i^p, \phi_i^p)\}_{i=1}^{i=N}$$

where with $a_{y_i}^p$ we denote vehicle lateral acceleration, with r_i^p yaw rate, with ϕ_i^p roll angle for an arbitrary but fixed point i.

Due to external and internal environment uncertainties and/or disturbances, there will be an offset random vector \mathbf{O} that will account for the difference between planned point and the realized. Here, the vector can be defined as

$$\mathbf{O} := [O_x, O_y, O_v, O_t, O_{a_y}, O_r, O_\phi].$$

Initially, before the beginning of the journey of a vehicle, the path that will be really taken, i.e. realized, will be unknown, i.e. random. Hence, the taken point i will in fact be random such that

$$(x_i^p + O_x, y_i^p + O_y, V_i^p + O_v, t_i^p + O_t, a_{y_i}^p + O_{a_y}, r_i^p + O_r, \phi_i^p + O_\phi).$$

And its realization is revealed only when the realizations of its offsets, i.e. vector \mathbf{o} , is known

$$(x_i^p + o_x, y_i^p + o_y, V_i^p + o_v, t_i^p + o_t, a_{y_i}^p + o_{a_y}, r_i^p + o_r, \phi_i^p + o_\phi).$$

Thus, from the perspective of an entire realized trajectory, in principle we may assume that each point in the planned trajectory experiences an offset which is i.i.d. realization from some multidimensional distribution that characterizes the offset uncertainty. However, not all marginal distributions of an offset distribution are relevant for occurrence of rollover.

There are multiple metrics (indices) that based on the vehicles' dynamical states can be used to detect or indicate the state of rollover. The most common rollover index is Load Transfer Ratio (LTR) which will be elaborated further in next sub-section. However, in order to explain the core mathematical conceptualization, it will suffice to consider LTR , at a particular vehicle speed V , i.e. LTR_V , as a function of state space spanned by lateral acceleration a_y , yaw rate r , and roll angle ϕ , thus $LTR_V = LTR(a_y, r, \phi; V)$, which, if above some fixed threshold TR indicates rollover occurrence. Thus, there is a subspace in the space of trajectories in which a rollover can occur. And, this can be mapped out by using LTR metric.

To put this all together let us consider a planned point $(x_i^p, y_i^p, V_i^p, t_i^p, a_{y_i}^p, r_i^p, \phi_i^p)$. The quantity of interest P_i is probability that given planned point will have its realization in rollover region, hence

$$P_i = P \left[LTR_{V_i^p}(a_{y_i}^p + O_{a_y}, r_i^p + O_r, \phi_i^p + O_\phi) > TR \right] = E \left[\mathbb{I}_{LTR_{V_i^p} > TR}(a_{y_i}^p + O_{a_y}, r_i^p + O_r, \phi_i^p + O_\phi) \right]$$

$$= \int f_o(o_{a_y}, o_r, o_\phi) \mathbb{I}_{LTR_{V_i^p} > TR}(a_{y_i}^p + o_{a_y}, r_i^p + o_r, \phi_i^p + o_\phi) da_y dr d\phi$$

where f_o is the density of the offset vector¹ and the main mathematical object to be characterized. Once this is done, to each planned point i there will be an associated probability P_i , numerically calculated, that true position will stay in rollover region.

Making the assumption of a fixed cost of rollover to be C , the distribution of losses L is then path point dependent and is of Bernoulli type such that, for planned point i loss variable L_i takes value C with the probability P_i or 0 with probability $1 - P_i$. Thus, in further discussions we will focus on characterizing P_i and in numerical examples make the choice of C .

Note: The cost C is either random variable or fixed value. In this work we will assume C have fixed value and that of the autonomous vehicle under consideration. Thus, we will assume that the total loss occurs in case of rollover. In principle, $C(\omega)$ can be a random variable which is a function of other random variables (for example: $F_1(\omega), F_2(\omega), \dots, F_n(\omega)$) that impact the value of cost (distribution) due to rollover, or even more general, it might be considered that $C_i(\omega) = C(i, F_1(\omega), F_2(\omega), \dots, F_n(\omega))$, i.e. C is random variable which

¹ In principle, the offset distribution may be speed dependent i.e. $f_o = f_o(V)$.

is addition path dependent. By focusing on probabilistically characterizing probabilities of rollover i.e. P_i 's in this work we develop general framework for loss distribution in case of rollover and the particular choice of cost in the event of rollover is left as a modeling choice within this framework which insurer can make based on past claims experience data. Thus, in a general setting, L_i takes value C_i with the probability P_i or 0 with probability $1 - P_i$, having the expected loss $E[L_i] = E[C_i]P_i$.

1.3 Rollover Index (RI)

Rollover is a type of vehicle crashes in which a vehicle tips over onto its side or roof. Vehicle rollover can be generally divided into two categories: tripped and untripped rollover. Tripped rollovers are caused by forces from an external object, such as a curb or a side wind. Untripped rollovers are the result of steering input, speed, and friction with the ground [6]. In our work, we only focused on untripped rollovers, which are triggered by internal vehicle dynamics.

In a more conservative sense of vehicle safety, vehicle rollover is considered as an inevitable consequence of tire lift-off. Therefore in most of the literature concerning rollover prediction and prevention, it is defined as the situation in which one side of the vehicle wheels are lifted off the ground.

Rollover prevention can be achieved by employing rollover warning (e.g. using warning signs of road curve/curb ahead, as shown in Figure 1, or visual signals or auditory alarms to warn the driver about potential rollover incidents [7]) and anti-rollover systems (using anti-roll bar [10] or vehicle dynamical control methods [8][9] to prevent rollover incidents).



Figure 1. Signs for warning curves with an increased danger of rollover (Google Image).

Most rollover warning systems in early 1990s were based on signal threshold techniques [11]-[14]. These systems turn on the warning actions (generate auditory alarms or display visual signs, e.g. a combination of static and fiber-optic warning message sign [15]) when the vehicle roll angle or the lateral acceleration exceeds a pre-selected threshold value. However, such thresholds are usually conservative and static. To prevent/reduce rollover, one of the most important enabling techniques is the development of accurate rollover threat indices.

Up to our knowledge this work is first to address the modeling of rollover risk probability for autonomous vehicles. Since the literature in automotive and vehicle control areas typically consider deterministic vehicle dynamics and environment conditions (see [6][9][18]-[20]), even with uncertainties, the probabilistic features of vehicle dynamics, especially for rollover, were rarely studied.

1.3.1 Load Transfer Ratio (LTR)

The load transfer ratio (LTR) is one of the most popular RIs, which, by the most common definition, is expressed as,

$$LTR = \frac{F_{z,right} - F_{z,left}}{F_{z,right} + F_{z,left}}$$

where $F_{z,right}$ and $F_{z,left}$ are the vertical tire load on the right and left sides of the vehicle, respectively.

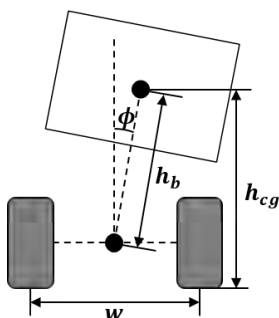


Figure 2. An example of vehicle roll dynamics model.

Due to the absence of effectively direct measurements of vertical tire loads, the LTR is usually estimated from other vehicle states, e.g., vehicle lateral acceleration, yaw rate, roll angle, etc. The LTR adopted in this work is based on the roll dynamics model shown in Figure 2, and can be expressed below, considering both simplicity and accuracy (see [16][17]),

$$LTR = f(V_x, a_y, r, \phi) = \frac{2h_{cg}(a_y + V_x r)}{w g} + \frac{h_b}{w} \phi \quad (1)$$

where h_{cg} is the height of center of gravity (CG), w the track width, h_b the distance from CG to roll center, g the acceleration of gravity, V_x the vehicle longitudinal speed, a_y the lateral acceleration, r the yaw rate, and ϕ the roll angle.

There are some alternative expressions of LTR in (1), e.g.,

(1) Rajamani (2011) [18]:

$$LTR = f(V_x, a_y, r, \phi) = \frac{2m_s(a_y + V_x r)h_b}{m g w} + \frac{2m_s h_b \tan \phi}{m w} \quad (2)$$

where m_s and m are the sprung mass and total mass of the vehicle;

(2) Larish et al.(2013) [19]:

$$LTR = f(V_x, a_y, r, \phi) = \frac{2h_b}{w} \frac{((a_y + V_x r) \cos \phi + (h_b r^2 + g) \sin \phi)}{g} \quad (3)$$

It is noteworthy that:

- (1) Most of these RIs are calculated by using the same set of key vehicle states, e.g. vehicle speed, lateral acceleration, yaw rate, roll angle, etc.
- (2) By assuming $m_s \approx m$, $h_b \approx h_{cg}$ and ϕ is relatively small, which are typically true for passenger cars (may not for commercial trucks), Equations (2) and (3) are actually consistent with Equation (1);
- (3) In our pipeline, the LTR is defined as an independent Matlab function, thus can be easily replaced by any RI mentioned above, if necessary.

Most importantly, LTR rollover index (see Equation (1)) induces a non-rollover region in the state space of (a_y, r, ϕ) , and an example, in a discretized fashion, for $V_x = 120\text{km/h}$ is shown in Figure 3. Simply, if during a course of traversing a trajectory at speed V_x , a vehicle keeps its state trajectory (a_y, r, ϕ) in blue colored region, rollover will not occur. However, when that is not the case there will be propensity of rollover. Importantly, for a given set of vehicle parameters, the rollover region is, in principle, depended on the vehicle speed V_x as shown in Figure 4 for a $V_x = 35\text{km/h}$ demonstration.

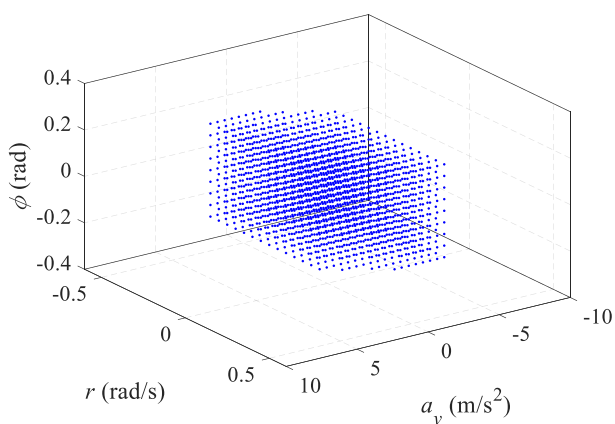


Figure 3. LTR induced non-rollover region ($V_x = 120\text{km/h}$)

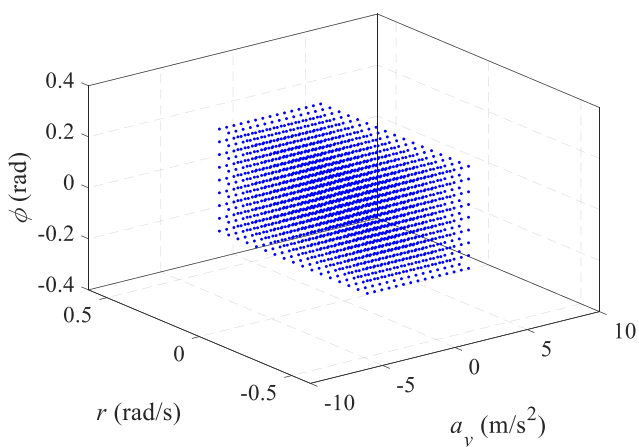


Figure 4. LTR induced non-rollover region ($V_x = 35\text{km/h}$)

1.3.2 Other Possible Indices

There are also some other RIs:

(1) Time-To-Rollover (TTR) metric;

Time-To-Rollover (TTR) metric was proposed in [21] and [22] to assess rollover threat. Ideally, the TTR metric is an accurate ‘count-down’ time towards rollover happening, which in turn indicate the level of rollover threat [22].

The procedure of TTR calculation is as shown in Figure 5. A yaw/roll dynamics model is required to predict vehicle dynamics response in response to steering input in real time. Based on this model, the TTR metric is defined as following: assuming the steering angle input stays fixed at its current level in the foreseeable future, the time it takes for the vehicle sprung mass to reach its critical value is defined as TTR.

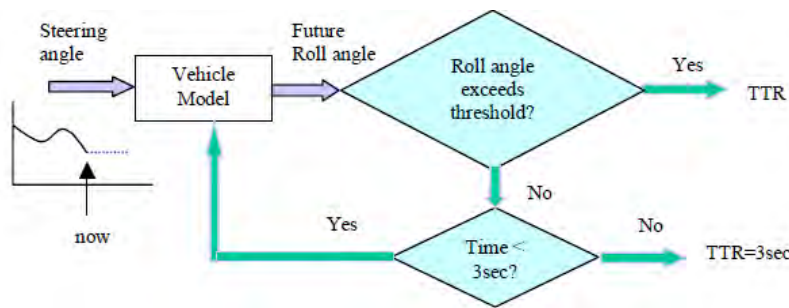


Figure 5. Flow chart for the TTR calculation [22].

TTR is a count-down time for future rollover, thus does not reflect vehicle rollover status at the current instant. And there are two major difficulties to implement this method:

- 1) The effectiveness of this metric highly depends on the accuracy of the adopted vehicle yaw/roll dynamics model. If the model is not accurate enough, then the vehicle roll angle cannot be predicted ahead of time.
- 2) The vehicle model also needs to be super-real-time (much faster than real time). For example, in order to predict a TTR of (up to) 3s, one needs to predict vehicle response in the next 3s repeatedly. If TTR is updated every 50ms, then the vehicle model needs to be 60 times faster than real-time.

The above dilemma of accuracy and efficiency can be solved by using techniques such as Neural Network (NN), however, it requires to be trained and verified under a variety of driving patterns.

(2) Energy-based index [23];

Based on the idea that a vehicle has the potential to rollover as long as the ‘lateral kinetic energy’ is not smaller than the minimum ‘required potential energy’, a rollover potentiality index Φ_0 is defined as,

$$\Phi_0 = \frac{1}{2} |V_x \beta|^2 - \sqrt{g^2 + a_y^2} \sqrt{\left(\frac{w}{2}\right)^2 + h_{cg}^2} + \frac{w}{2} a_y + h_{cg} g$$

where β is the vehicle sideslip angle. This developed rollover index can be implemented on vehicles with Electronic Stability Program (ESP) with/without extra roll rate sensor. However, an accurate on-line estimation of vehicle sideslip angle is required but difficult to achieve.

(3) Mass-Center-Position (MCP) metric [24][25];

MCP metric is a novel index for both tripped and untripped rollover which considers the geometric relationship between vehicle’s sprung and unsprung masses. The index adopts two vehicle roll dynamics models for estimating vehicle rollover status before and after tire lift-off, respectively. For detailed formulation, please refer to [24] and [25].

This index is an extension to traditional LTR, by continuously providing roll motion estimation even after tire lift-off, thus can tell the difference between actual vehicle rollover and tire lift-off. However, despite of the merits, its major difficulty of implementation is requiring measurement or estimation of the position and movement of unsprung mass.

1.3.3 Notes of Caution

The rollover index LTR adopted in this work is based on the so-called pendulum model, which considers the vehicle as a mass point with roll motion as an extra degree of freedom. This simplified model works better with vehicles with relatively compacted physical structures and rigid suspension systems (such as SUVs) since the impact of suspension deformation on roll dynamics are neglected.

However, for heavy-duty trucks and articulated trucks, the complex dynamic characteristics of the suspension system or articulated mechanism may not be ignored; thus, more involved system analysis, subject to future research, is required for accurate rollover prediction/estimation.

Section 2: Critical Maneuvers and Main Perturbances

In this section, what the critical maneuvers are, what are their key determinants, and how they can be seen from time evolution and state space perspective will be discussed. We also introduce three types of perturbances that can affect the execution of critical maneuvers and thus affect the time evolution of the state space.

2.1 Critical Maneuvers

The rollover incidents are basically generated by aggressive vehicle roll motion triggered by vehicle lateral dynamics, e.g. steering input. In [22], a set of maneuvers was selected, which can cover a wide range of rollover or near-rollover incidents, as shown in Figure 6. Those maneuvers can be classified into four patterns: ramp steering, ramp entering, obstacle avoidance, and “worst-case” maneuvers.

In our work, the maneuver selection follows such a classification. High-speed cornering is corresponding to Ramp entering, single lane change and double lane change are corresponding to obstacle avoidance, and fishhook is corresponding to the worst-case maneuver.

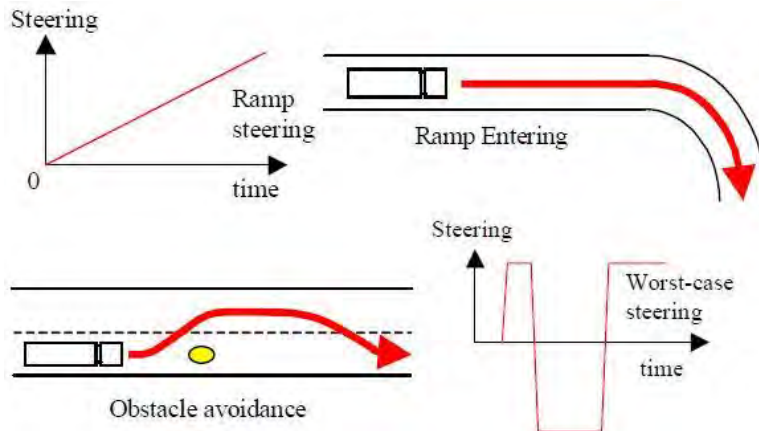


Figure 6. Four types of maneuvers to trigger most of the rollover incidents [22].

Specifically, fishhook and ramp steering are both maneuvers to intentionally trigger rollover, which are not typical for real world driving. Therefore, the high speed cornering, single lane change, and double lane change maneuvers are adopted as the representative maneuvers for rollover evaluations.

Throughout this work, we will assume that an autonomous vehicle keeps the constant speed V_x throughout the selected maneuvers. The rationale for this is mainly economic and does not affect the generality of this work.

Keeping the speed constant, through maneuvers, the autonomous vehicle, during the time of maneuver, has to appropriately change its lateral acceleration a_y , yaw rate r , and roll angle ϕ .

2.1.1 High-speed Cornering (HSC) Maneuver

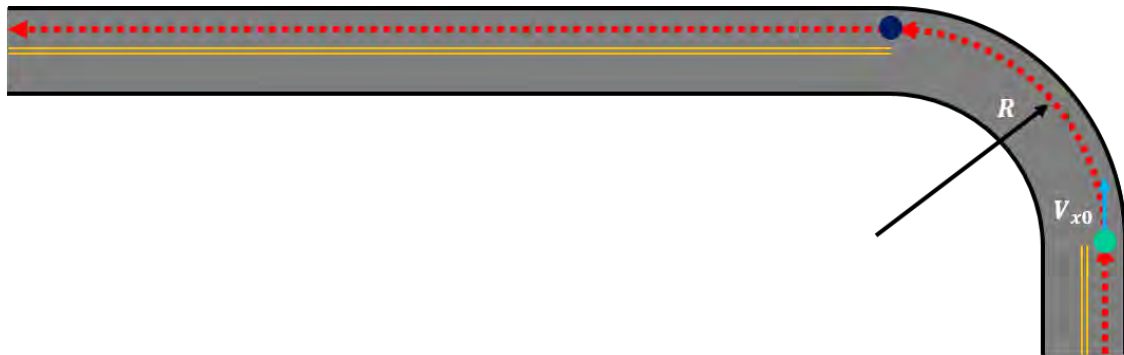


Figure 7. HSC maneuver

High-speed cornering is a maneuver where the vehicle turns along the curve at a high speed, as depicted in Figure 7, which is commonly happening at intersections or when vehicles are entering ramps. The radius R of the road curve is the main geometric characteristic of this maneuver. In this work, the stylized values of $R = 300\text{m}$ are considered to represent a “sharp” corner, while for $R = 1000\text{m}$ they represent “normal” corner.

When traversing at the given constant speed (for example $V_x = 120\text{km/h}$ given $R = 1000\text{m}$), an ideal vehicle, regardless of internal or external conditions, governed by an ideal controller, performing this maneuver, would across time exhibit evolution of lateral acceleration a_y , yaw rate r and roll angle ϕ as presented in Figure 8.

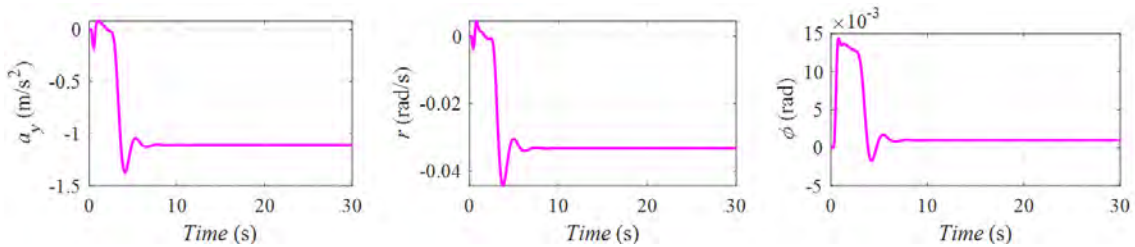


Figure 8. HSC time-domain response ($V_x = 120\text{km/h}$, $R = 1000\text{m}$).

From another perspective, in the state space (a_y, r, ϕ) , this vehicle performing the same maneuver would trace the state trajectory presented in Figure 9. Here, as the vehicle travels, the starting and ending point in the state space is the origin point $(0,0,0)$, and the vehicle can revisit several times the same point in the state space during its travel.

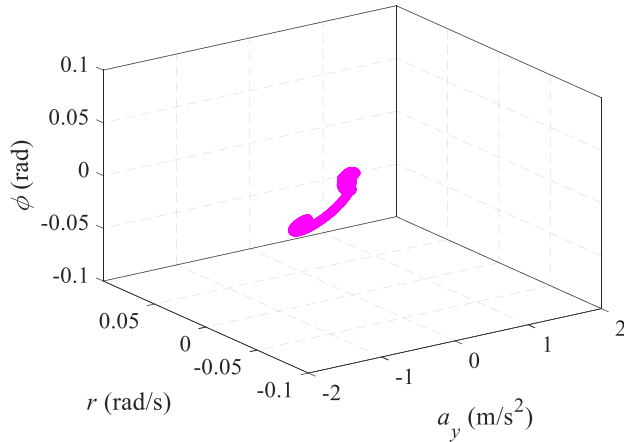


Figure 9. HSC vehicle state trajectory ($V_x = 120\text{km/h}$, $R = 1000\text{m}$).

2.1.1.2 Single Lane Change (SLC) Maneuver

Single lane change is a maneuver where a driver changes from one lane to another as depicted in Figure 10. The length L in which the maneuver takes place is the main geometric characteristic of this maneuver. Given the same speed, to mimic the “normal” driving style, we assume $L = 70\text{m}$ while for “aggressive” driving $L = 30\text{m}$. In Figure 10, the (standard) 3.7m for the lateral offset (which equals the distance between the center lines of the two adjacent lanes) is given.

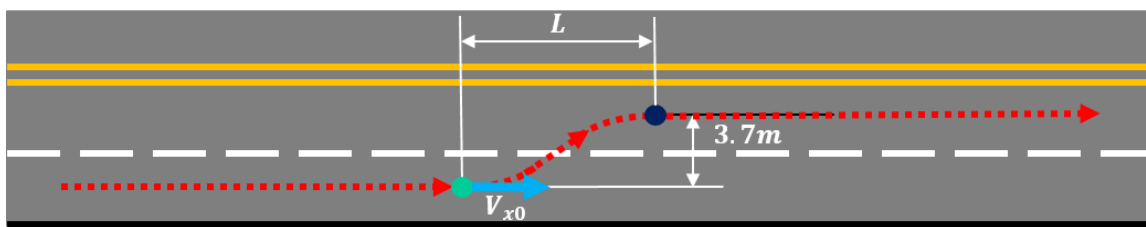


Figure 10. SLC maneuver.

When driving at the given constant speed (for example $V_x = 120\text{km/h}$ given $L = 70\text{m}$), an ideal vehicle, regardless of internal or external conditions, governed by an ideal controller, performing this maneuver, would across time exhibit evolution of lateral acceleration a_y , yaw rate r and roll angle ϕ as presented in Figure 11.

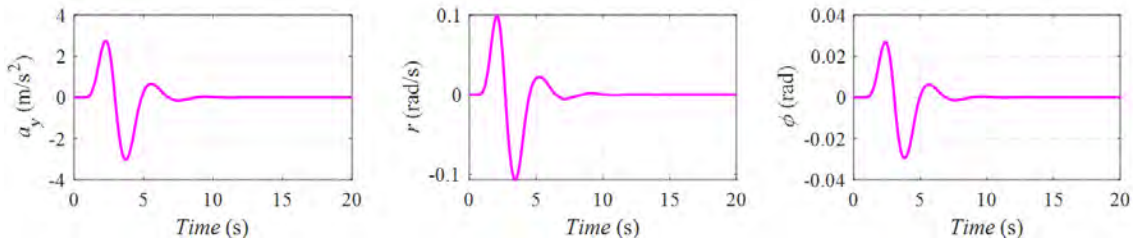


Figure 11. SLC time-domain response ($V_x = 120\text{km/h}$, $L = 70\text{m}$).

From another perspective, in the state space (a_y, r, ϕ) , this vehicle performing the same maneuver, would trace the state trajectory presented in the Figure 12.

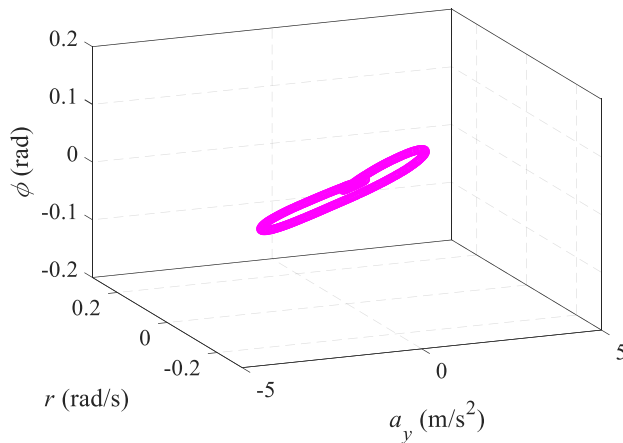


Figure 12. SLC vehicle state trajectory ($V_x = 120\text{km/h}$, $L = 70\text{m}$).

2.1.3 Double Lane Change (DLC) Maneuver

Double lane change is a maneuver where a driver changes from one lane to another and then returns back to the initial lane, as depicted in Figure 13. The length L in which the maneuver takes place is the main geometric characteristic of this maneuver. Given the same speed, to mimic the “normal” driving style, we assume $L = 150\text{m}$ while for “aggressive” driving $L = 70\text{m}$. In Figure 13, the (standard) 3.7m for the lateral offset (which equals the distance between the center lines of the two adjacent lanes) is given.

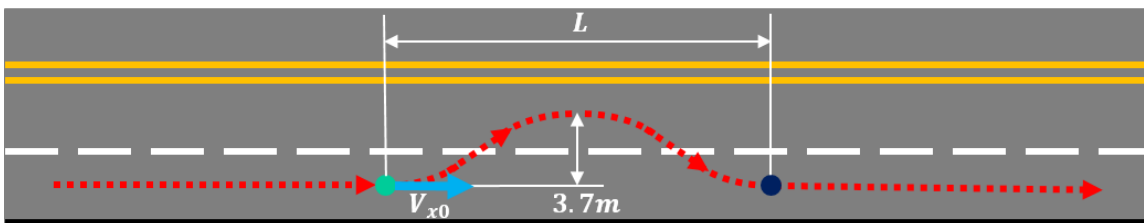


Figure 13. DLC maneuver

When driving at the given constant speed (for example $V_x = 80\text{km/h}$ given $L = 150\text{m}$), an ideal vehicle, regardless of internal or external conditions, governed by an ideal controller, performing this maneuver, would across time exhibit evolution of lateral acceleration a_y , yaw rate r and roll angle ϕ as presented in Figure 14.

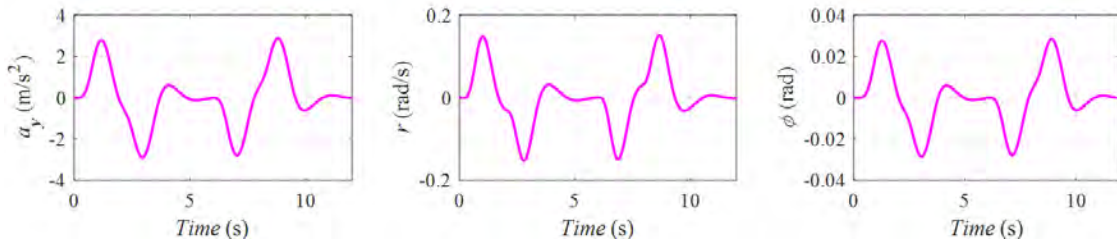


Figure 14. DLC time-domain response ($V_x = 80\text{km/h}$, $L = 150\text{m}$).

From another perspective, in the state space (a_y, r, ϕ), this vehicle performing the same maneuver, would trace the state trajectory presented in the Figure 15.

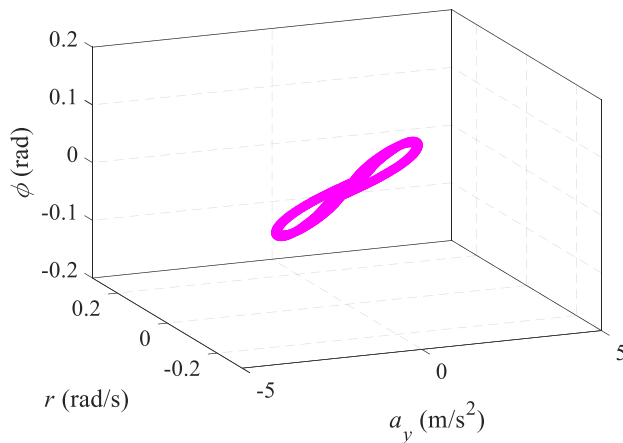


Figure 15. DLC vehicle state trajectory ($V_x = 80\text{km/h}$, $L = 150\text{m}$).

2.2 Main Perturbances

The three main sources of perturbances that we investigated are sensors, controllers, and environmental factors.

2.2.1 Sensor

The sensor noise can introduce uncertainty to vehicle states, which may, in turn, affect the calculation result of rollover probability and loss modeling. Bias Stability (also known as Bias Instability) can be defined as how much deviation or drift the sensor has from its mean value. With high-end sensors, the vehicle states can be accurately measured. For example, the bias stability for lateral acceleration measurement can be as low as $5\mu\text{g } 1\sigma$, and $0.01^\circ/\text{s } 1\sigma$ for yaw rate, and $0.05^\circ 1\sigma$ for roll angle, as is the case for the vehicle under consideration in this work. For this reason, we do not include sensor noise in our considerations in this work and deem it to be negligible.

2.2.2 Controller

The controller used in Simulation is the embedded CarSim driver model, which is a delicately designed and optimally tuned PID-based controller for path following control, tracking control, braking control, vehicle stability control, and other customized control tasks (e.g. tracking predefined steering input).

This controller can consistently achieve expert level of driving performance in various kinds of driving situations, thus it is a good representation for mimicking the existing autonomous driving systems. Specifically, this controller uses PID-based techniques for multi-objective tracking control, which is typical for tracking controller design in the industry. Thus the main reason why this embedded controller is selected is that it is well designed to achieve good performances in both path tracking and speed tracking at the same time.

In principle, if we adopt some other external/self-designed controllers, it would differently impact perturbances. However, from a practical point of view, it would not affect the generality of the analysis presented in this report. The controller choice is thus kept consistent through this report, and for other choices of controllers, all results would have to be redone.

Note: The reader should note that an ideal controller, i.e. the controller which would execute, at every moment in time, an ideal state of lateral acceleration a_y , yaw rate r , and roll angle ϕ , under every condition, for every maneuver (traced pink trajectories in Figures 9.,12. and 15. for example) does not exist. In fact, in an autonomous driving system design, the ultimate goal of the controller is to track the planned path and speed profile as accurate as possible. However, for the simplicity of hardware implementation and computational considerations, the reference model for controller design cannot fully take into account the complexity and nonlinearity of vehicle dynamics characteristics as well as environmental perturbation. In addition, the lateral acceleration a_y and the yaw rate r are considered as the primary control objectives for most controllers, whereas the roll angle ϕ is often overlooked. Therefore, the real controllers, though generally are capable of presenting good tracking performances, cannot entirely prevent the autonomous vehicle deviating from the desired trajectories.

2.2.3 Environmental Factors

For a given tire, the normalized traction force is defined as,

$$\mu = \frac{\sqrt{F_x^2 + F_y^2}}{F_z} \tag{4}$$

where F_x , F_y , and F_z are longitudinal, lateral and vertical tire forces, respectively. The tire-road friction coefficient (TRFC) is defined as the maximum value of μ [29], which determines the maximum force that the tire can supply.

TRFC can significantly affect the longitudinal, lateral, yaw, and roll behaviors of the vehicle. Therefore, the real-time TRFC estimation has always been an important subject for vehicle active stability and safety control system design. In our case, the uncertainty of TRFC will affect the autonomous driving systems predicting the vehicle roll motion. Particularly, with an inaccurate estimation of TRFC, the autonomous vehicle may suffer from a rollover accident, due to excessively planned steering maneuver during a critical high-speed collision avoidance.

In our work, the tire-road friction condition is generally divided into three categories: low- μ (0.2-0.4, e.g. icy road), mid- μ (0.4-0.7, e.g. mildly wet asphalt road) and high- μ (0.7-1.0, dry asphalt road).²

Aside from TRFC, a side wind can be an environmental factor which influences the vehicle stability. In the field of vehicle dynamics control, a side wind is not particularly involved, and even when considered, is treated as a local-scale and short-term system disturbance. Such a disturbance only has a temporary impact on vehicle behaviors (see [26]-[28]). Therefore, the modeling of side wind is generally simplified as an extra bounded step (or impulsive) input of the vehicle system. However, in the case of large-scale trajectory planning, such an influence is basically highly transient, and difficult to be accurately modeled and predicted in advance, thus not considered in this work.

Exact values of TRFC are very difficult to gauge for a particular stretch of the road. There are a few studies developing different TRFC estimation methods [30]:

- (1) Experimental-based methods (expensive, difficult to process data): Optical sensors and cameras (medium accuracy, medium repeatability), Acoustic sensor (medium accuracy, low repeatability) and Tire tread sensor (high accuracy, medium repeatability);
- (2) Model-based methods (a priori knowledge is required for modeling): Wheel and vehicle dynamics based (high accuracy, high repeatability), Tire model based (high accuracy, medium repeatability) and Slip-slope based (medium accuracy, low repeatability).

Section 3: Mixture Model for Offset Distribution

In this Section, to account for all sources of perturbation that can eventually create an offset distribution we resort to creating a mixture model of perturbances.

3.1 Dependence of Offset on the Maneuver Type, Road Type and Speed

In principle, the offset distribution is dependent on maneuver type, road type, and vehicle speed. That would not be true if the autonomous vehicle would possess an ideal controller. However, since that is never the case, keeping the same controller, speed, and road type, different maneuvers will pose different challenges to the controller, and the nature of offset exhibited will be different. Here, offset is, as discussed, seen as a difference between the planned vehicle dynamical state and realized one. Similarly, keeping all else the same, having different speeds while performing maneuvers under the same road conditions will task controller more and change the nature of the offset. Finally, by changing road conditions, more or less pressure could be put on the controller's performance. For example, slippery road tasks controller more than a dry road, keeping all other things the same. These insights will be guiding the development of our offset distribution. Here, with f_{ijk} we will denote the offset distribution for case of maneuver i , road type j , and speed level k .

3.2 Formulating a Mixture Model

In principle, every trajectory that autonomous vehicle can travel can be seen as a mixture of maneuvers taken, road types traveled, and speed levels had. Such a view naturally invokes the use of mixture distributional models as an overall model for an offset on the level of trajectory. Thus, we will define the offset distribution as

$$f_o(o_{a_y}, o_r, o_\phi) := \sum_{ijk} \pi_{ijk} f_{ijk}(o_{a_y}, o_r, o_\phi)$$

where π_{ijk} denotes the percentage of trajectory where maneuver i , road type j and speed level k were observed, and $f_{ijk}(o_{a_y}, o_r, o_\phi)$ is offset distribution of those circumstances, as described in sub-chapter above. Note that, this modeling approach assumes that driving in straight line possess no rollover risk.

Note: The mixture weights π_{ijk} can be a priori set in trajectory planning or, estimated in simulations of traffic flow scenarios. The former is not considered in this work, and the latter is the approach that will be taken.

Now, we will make further assumption that will simplify our analysis with no loss of generality of the entire approach in this work.

Assumption 1: The offsets across lateral acceleration a_y , yaw rate r , and roll angle ϕ are independent. Hence, the density function $f_{ijk}(o_{a_y}, o_r, o_\phi)$ is the product of density functions $f_{ijk}(o_{a_y})$, $f_{ijk}(o_r)$ and $f_{ijk}(o_\phi)$.

Here, the challenge that remains is to find the model for each of $f_{ijk}(o_{a_y})$, $f_{ijk}(o_r)$ and $f_{ijk}(o_\phi)$ and properly parametrize it.

3.3 Using CarSim Software to Discover the Component or (sub-) Distributions

Developed by Mechanical Simulation Corporation (MSC), CarSim is a multi-body-dynamics-based simulation software that delivers accurate, detailed, and efficient methods for simulating the performance of passenger vehicles and light-duty trucks. The CarSim software has decades of real-world validation by automotive engineers and as such is universally the preferred tool for analyzing vehicle dynamics, developing active controllers, calculating a car’s performance characteristics.

The Dynamic Systems and Control Laboratory (DSCL) at ASU purchased CarSim license and has been conducting various research on vehicle system dynamics and control, as well as developing the autonomous driving technologies by using this software.

We set vehicle specifications in CarSim software to correspond to the vehicle available in the lab and describe them in detail in the final section.

Given that autonomous vehicles are very expensive equipment, from a practical perspective, they cannot be used to generate enough observations to calibrate each component distribution effectively. For this purpose, we will use CarSim software, as schematically depicted in Figure 16.

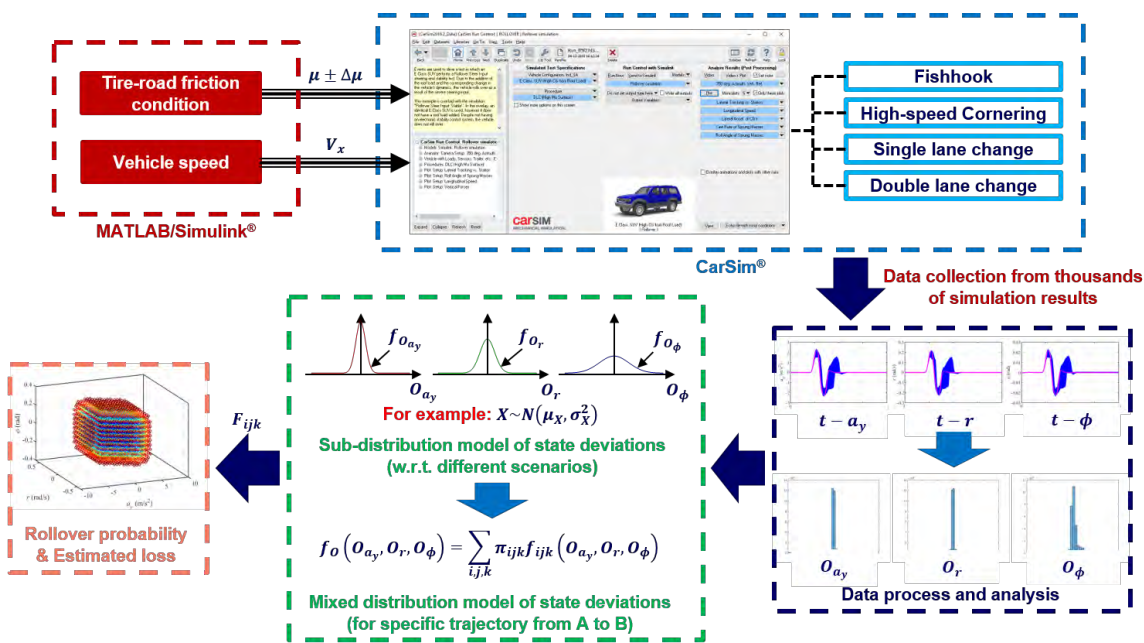


Figure 16. Using CarSim software to characterize the component distribution of a mixture model

In a given scenario, as an input to CarSim software, we will sample TRFC value from a given tire road friction interval to determine road type, choose vehicle speed, choose maneuver, and values that govern the vehicle geometry. We will task the CarSim software to trace the lateral acceleration a_y , yaw rate r , and roll angle ϕ evolution in time. We will repeat this process for the prescribed number of times. The result of this procedure are time dependent histograms of the lateral acceleration a_y , yaw rate r , and roll angle ϕ which are depicted in Figure 16 in a simplified manner and colored in blue (lower section, right-hand box). Based on them, a sufficient amount of information is available to calibrate a component distribution as we have multiple realization of planned (pink) and realized state (blue) for each time index. However, to simplify this process, in addition to Assumption 1, we will make an assumption below.

Assumption 2: For a given state variable (a_y , r , or ϕ) we will define an aggregate empirical offset distribution to be a collection of all offset realization regardless of their time indices.

Simply put, with Assumption 2, we collapse the time dimension of offset distribution and look at all offset realizations together.

Note: Assumption 2 is justifiable as it represents a conservative choice relevant for the insurer. Across time index, there is one empirical offset distributions that stochastically dominates all other. By collapsing time index, the stochastically dominating offset distribution will be subsumed in the aggregate offset distribution.

Note: Though Assumption 1 can be more nuanced, from the practical point of view of this work, it represents a good trade-off between complexity and accuracy. Instead of assuming independence between lateral acceleration, yaw rate, and roll angle offsets, one can use three-variate distributions, and based on simulation results, perform its fit. That would be more accurate, but in practice, more computationally intensive. The final assumption needed before we embark on investigation of specific component distribution is assumption of their distributional type.

Assumption 3: All component distributions are of three variate normal type constructed as a product of three independent univariate normal distributions.

Specifically, with Assumption 3, we assume that $f_{ijk}(o_{a_y})$, $f_{ijk}(o_r)$, and $f_{ijk}(o_\phi)$ are mutually independent and follow a normal distribution. The main reason this assumption is made is modeling simplicity. A more nuanced approach is by no means impossible, but here it was deemed that it would not benefit the presentation of overall methodology and would detract the reader from its overall structure.

3.4 Simulation and Experimental Results

Now, we consider $3 \times 3 \times 4 = 36$ component distribution for mixture distribution model to deal with any imaginable trajectory. Specifically, they will correspond to three scenarios for maneuvers, three scenarios for road type and four speed ranges. Intervals for speed [kph] scenarios are chosen such that they correspond to ranges relevant for beginning or stopping of driving (0-35), urban driving conditions (35-50), rural driving conditions (50-80) and highway driving conditions (80-100 or 120). Speed levels are chosen to be endpoints of the intervals because the offset distributions for the highest speed in a given interval will stochastically dominate all other distributions for lower speeds within the same interval. From insurer’s perspective, these are most conservative offset distributions for a given interval. Hence, for our purposes, the definitions of scenarios for sub-distribution models are:

- Maneuvers (i) = [1: High Speed Cornering, 2: Single Lane Change, 3: Double Lane Change];
- Road type (j) = [1: LOW (mean = 0.3), 2: MID (mean = 0.55), 3: HIGH (mean = 0.85)];
- Speed [kph] (k) = [1: Start/Stop (35), 2: Urban (50) , 3: Rural (80) , 4: Highway (100 or 120)].

To include the varying road conditions, we will not keep TRFC constant but vary it within certain range variation by sampling it from uniform distribution. Here, we assume

- LOW range: $\mu=0.3 \pm 0.1$
- MID range: $\mu=0.55 \pm 0.15$
- HIGH range: $\mu=0.85 \pm 0.15$

Now, for each scenario, a component model can be obtained via analysis of simulation data using MATLAB/Simulink-CarSim. Per scenario, thousand sampling repetitions were made. The data processing time was approximately 20-30 minutes for each scenario.

The simulation results of various settings are summarized in Figure 17. Here, the differences between the preplanned directives and what has really materialized, under the chosen experiment settings, have been given in the context of our model. Specifically, the parameters of component distributions in a mixture model, having maneuver settings (increasing from non-aggressive to aggressive) for high speed cornering (HSC), single lane change (SLC), double lane change (DLC), and three road conditions (Low, Mid and High), are given. By using those, a loss distribution for any trajectory can be articulated. Further, as an example, by comparing the results of DLC, Low (friction coefficient) with $V_x = 100$ to $V_x = 35$, one can see that, when it comes to lateral acceleration a_y , distribution of differences between preplanned directives and executed ones, having standard deviations $\sigma_{ay} = 1.3142$ vs. $\sigma_{ay} = 0.0484$ respectively, is wider for higher speed, as expected. The analogous conclusion translates to other friction coefficients. Additionally, one can see that for DLC, Low with $V_x = 100$ case, moving from Low, Mid to High, we have standard deviations to be $\sigma_{ay} = 1.3142$, $\sigma_{ay} = 1.8315$ and $\sigma_{ay} = 2.415$ respectively. These results match the intuition in automotive science as it is known that dry roads, as opposed to wet, provide more traction and thus enable the lateral accelerations needed for rollover; thus, in essence being more dangerous.

$X \sim N(\mu_x, \sigma_x^2)$		Low			Mid			High		
		$(\mu_{o_{ay}}, \sigma_{o_{ay}})$	$(\mu_{o_r}, \sigma_{o_r})$	$(\mu_{o_\phi}, \sigma_{o_\phi})$	$(\mu_{o_{ay}}, \sigma_{o_{ay}})$	$(\mu_{o_r}, \sigma_{o_r})$	$(\mu_{o_\phi}, \sigma_{o_\phi})$	$(\mu_{o_{ay}}, \sigma_{o_{ay}})$	$(\mu_{o_r}, \sigma_{o_r})$	$(\mu_{o_\phi}, \sigma_{o_\phi})$
HSC	$V_x = 35$	(0,0)	(0,0)	(0,0)	(0,0)	(0,0)	(0,0)	(0,0)	(0,0)	(0,0)
	$V_x = 50$	(0,0.0002)	(0,0)	(0,0)	(0,0.0001)	(0,0)	(0,0)	(0,0.0001)	(0,0)	(0,0)
	$V_x = 80$	(0,0.0862)	(0,0.0041)	(0,0.0028)	(0,0.0016)	(0,0.0001)	(0,0)	(0,0.0006)	(0,0)	(0,0)
	$V_x = 120$	(0,0.37)	(0,0.0122)	(0,0.0036)	(0,1.6661)	(0,0.0764)	(0,0.0184)	(0,0.0223)	(0,0.0013)	(0,0.0003)
SLC	$V_x = 35$	(0,0.0004)	(0,0.0001)	(0,0)	(0,0.0002)	(0,0)	(0,0)	(0,0.0001)	(0,0)	(0,0)
	$V_x = 50$	(0,0.0097)	(0,0.0007)	(0,0.0001)	(0,0.0011)	(0,0.0001)	(0,0)	(0,0.0004)	(0,0)	(0,0)
	$V_x = 80$	(0,0.3390)	(0,0.0179)	(0,0.0033)	(0,0.0244)	(0,0.0014)	(0,0.0002)	(0,0.0033)	(0,0.0002)	(0,0)
	$V_x = 120$	(0,0.4595)	(0,0.0197)	(0,0.0044)	(0,0.1105)	(0,0.0038)	(0,0.0011)	(0,0.0113)	(0,0.0006)	(0,0.0001)
DLC	$V_x = 35$	(0,0.0484)	(0,0.0048)	(0,0.0005)	(0,0.0015)	(0,0.0002)	(0,0)	(0,0.0007)	(0,0)	(0,0)
	$V_x = 50$	(0,0.61)	(0,0.0492)	(0,0.0061)	(0,0.0548)	(0,0.0041)	(0,0.0005)	(0,0.0042)	(0,0.0004)	(0,0)
	$V_x = 80$	(0,1.2121)	(0,0.0921)	(0,0.012)	(0,1.18)	(0,0.11)	(0,0.0119)	(0,0.2553)	(0,0.0163)	(0,0.0027)
	$V_x = 100$	(0,1.3142)	(0,0.1298)	(0,0.0127)	(0,1.8315)	(0,0.2146)	(0,0.0181)	(0,2.415)	(0,0.3859)	(0,0.0249)

Figure 17. Parameters of component distributions in a mixture model having maneuver settings for sharp corner and aggressive driving.

Partial justification of Assumption 3 is given with QQ plots for each scenario and presented in Appendix A.

As an illustration, the examples of simulation results for two scenarios (SLC and DLC) are presented in Figures 18-19. The blue shaded regions represent traces of 1000 simulations while with pink color an ideal controller response is traced.

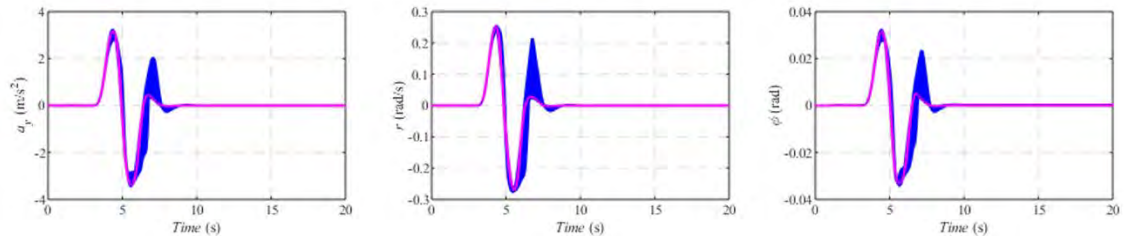


Figure 18. SLC simulation results MID ($V_x = 50\text{km/h}$, $L = 30\text{m}$)

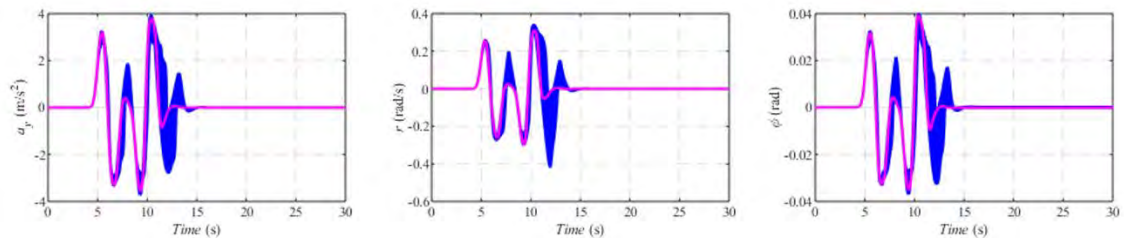


Figure 19. DLC simulation results MID ($V_x = 50\text{km/h}$, $L = 30\text{m}$)

Since the experimental vehicle, due to its value and practical feasibility, cannot be repeatedly placed in situations of high rollover risk, its place will be taken by the CarSim simulated vehicle. Having this in mind, in a way, the figures above show an evaluation of the differences between the preplanned trajectories for the car and what has really materialized during the execution of the experience.

Section 4: Integration with Google Maps

In this section, we integrate the developed methodology with Google Maps to evaluate the rollover probabilities/losses for autonomous vehicles in real-world situations. Two types of driving strategies are simulated, respectively. One is an aggressive driving strategy that represents the behaviors of autonomous vehicles under critical conditions such as emergent collision avoidance. The other is a normal/peaceful driving style, which represents the behavior of autonomous vehicles under non-critical/routine situations.

We will assume that in a rollover, the entire value of a vehicle is lost, i.e. total damage occurs. For stylized, but realistic setting, for the value of the autonomous vehicle, we take to be $C=50,000$ USD.

4.1 Route 1: Aggressive Driving Strategy

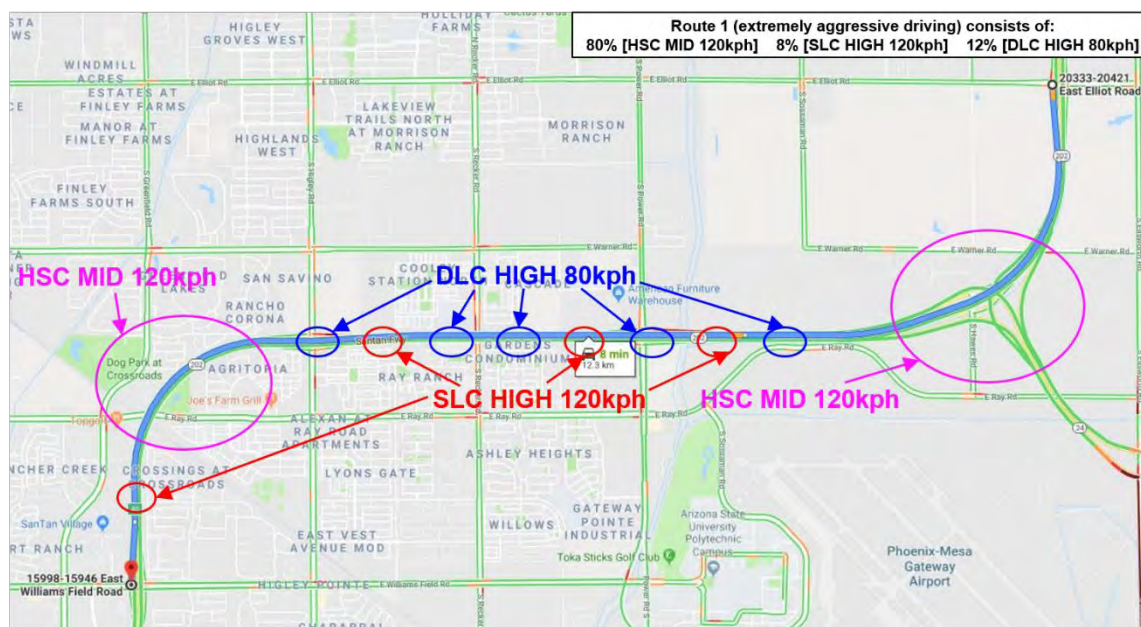


Figure 20. Planning of Route 1 by using Google Maps.

In this simulation case, the task is to evaluate the rollover probability and consequent loss when the autonomous vehicle plans to travel from 20333 E Elliot Road to 15998 E Williams Field Road through 202 high way in the area of Gilbert-Mesa cities. During the journey, multiple critical collision avoidance maneuvers will be required.

Firstly, a route from the starting point to the final point of destination is planned by using Google Maps, as shown in Figure 20. The route inherently consists of 2 large-radius cornering scenarios, which are highlighted in pink circles. The route coordinates are exported as *.kml file.

The route coordinate file is then processed, and the route coordinates are extracted and imported into CarSim. To make journey riskier, several high-potential emergent collisions are assumed and assigned along this route. Thus the autonomous vehicle has to fulfill multiple aggressive single and double lane changes, highlighted by red and blue circles, respectively. Consequently, the path for simulation is fully defined. Also, the speed profile can be roughly determined according to the speed limit with respect to the planned route.

In this case, the vehicle speed is 80km/h for double lane change maneuver, and 120km/h otherwise.

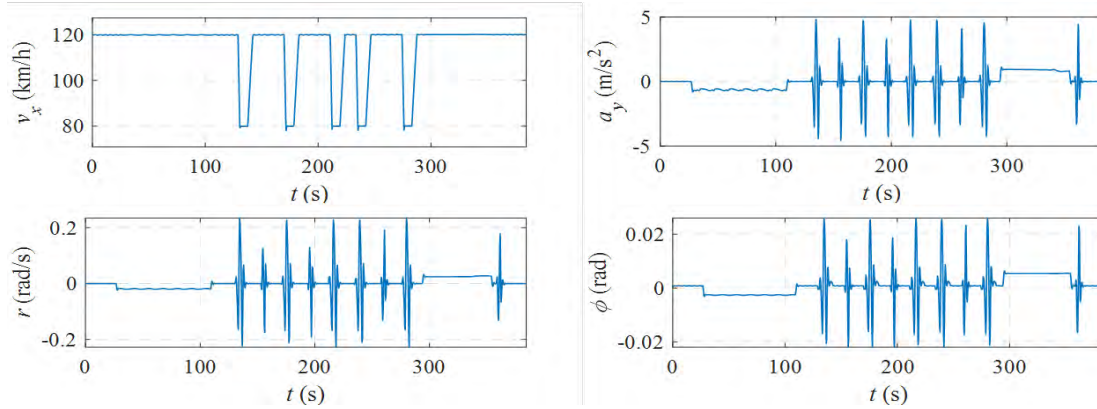


Figure 21. Simulated vehicle dynamics responses for Route 1.

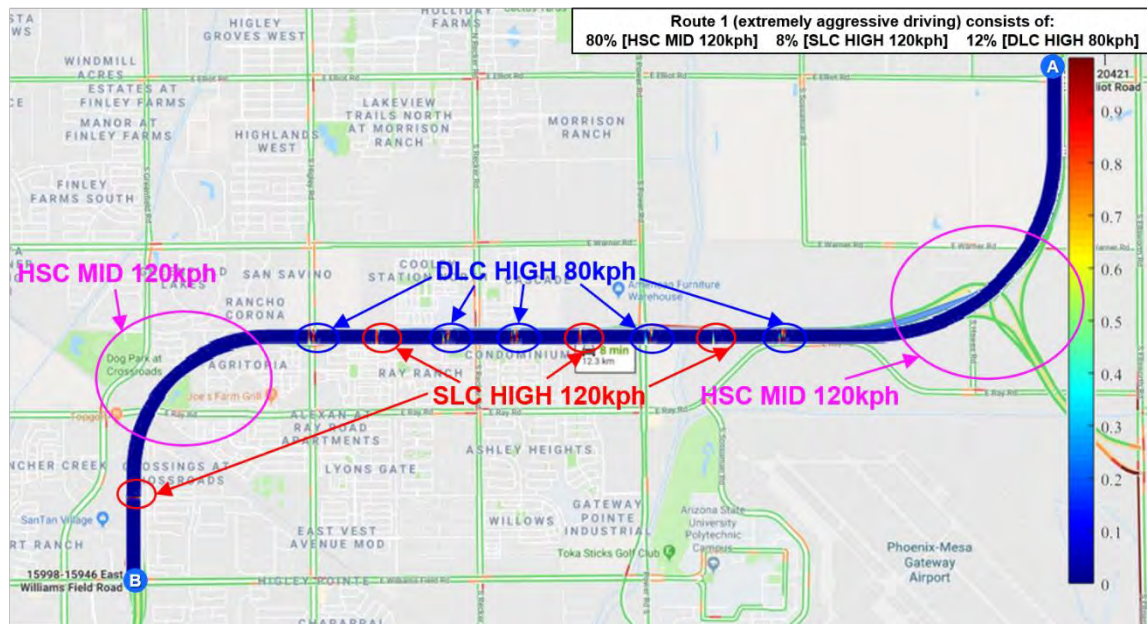


Figure 22. Simulation result of calculated rollover probability along the Route 1.

The simulation is conducted to predict the vehicle dynamics responses in the environment of CarSim-Matlab/Simulink. Specifically, CarSim provides the vehicle model, the controller (embedded driver model) and the established simulation scenario, while Matlab/Simulink is responsible for data collection and processing. The simulated vehicle dynamics responses are as shown in Figure 21. As shown in the figure, as the aggressive driving strategy is applied, large magnitude of a_y , r , and ϕ can be observed corresponding to each of the lane change maneuvers. Given that the vehicle traverses the state space of a_y , r , and ϕ having different speeds, the presented rollover region is for $V_x = 120$ kph as the most conservative choice. With bold dots, the trajectory the vehicle travels in the state space is embedded in the rollover region.

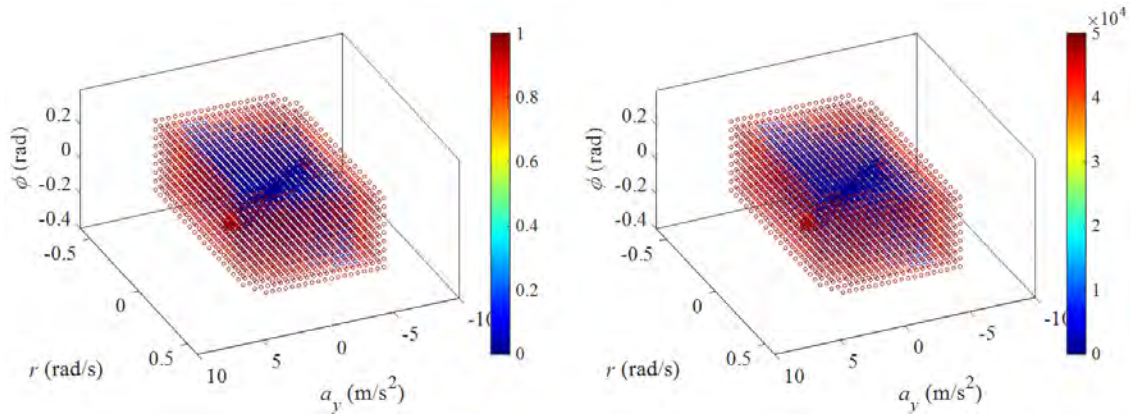


Figure 23. Simulation result of calculated rollover probability (left) and expected loss (right) in state space for Route 1. The rollover region is $V_x = 120$ kph.

Based on the predicted vehicle dynamics responses, the developed methodology is applied for rollover probability evaluation. The resulting rollover probability along the route is, as shown in Figure 22. Also, the rollover probability and expected loss with respect to the vehicle state trajectory in the 3-D state space (a_y, r, ϕ) are as shown in Figure 23. (bold blue and red dots mainly embedded in the rollover region).

The developed methodology allows for the assessment of the probability or rollover risk at every point of the trajectory. As shown in Figure 22, the high rollover probability (dark red) can be observed when the vehicle makes aggressive lane change maneuvers, which is consistent with the peaks of the vehicle dynamics responses in Figure 21. For example, the probability of rollover can reach ranges from 0.75 to 0.95 in the case of SLC. In addition, a very small safe/rollover-free region (in blue) is observed in Figure 23, while a large part of vehicle states are beyond these safe boundaries (bold red dots mainly embedded in the rollover region). The result indicates that the rollover probability of the route could be very high for autonomous vehicles if the aggressive driving strategy has to be applied.

To more clearly illustrate the relationship between the trajectory in the state space (bold blue and red dots), which the vehicle takes in the rollover region, we show the following three separate 2-dimensional cases. In Figure 24, we present the vehicle trajectory in the state space together with an aspect of the rollover region when $\phi = 0$. Similarly, in Figure 25, we present the vehicle trajectory in the state space together with an aspect of the rollover region when $a_y = 0$. Finally, Figure 26 presents the vehicle trajectory in the state space together with an aspect of the rollover region when $r = 0$. Similar examples can be made for other choices of a_y, r , and ϕ . As the sampling scheme becomes more refined, the graduation of probabilities becomes more apparent - however, the computational effort increases.

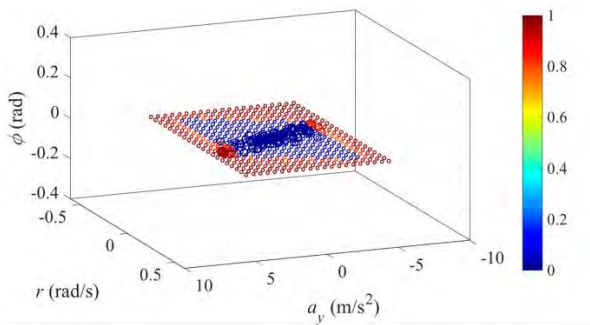


Figure 24. The $\phi=0$ plane.

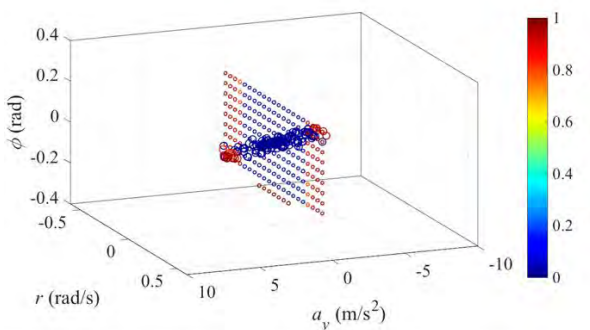


Figure 25. The $a_y=0$ plane.

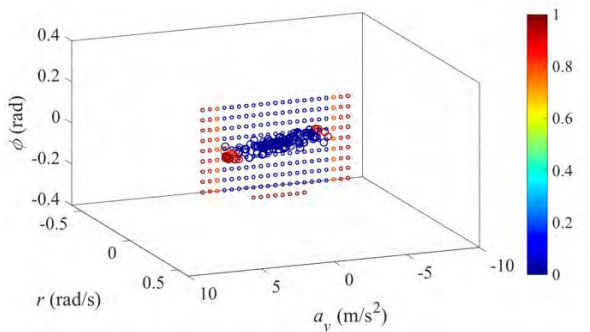


Figure 26. The $r=0$ plane.

4.2 Route 2: Normal Driving Strategy

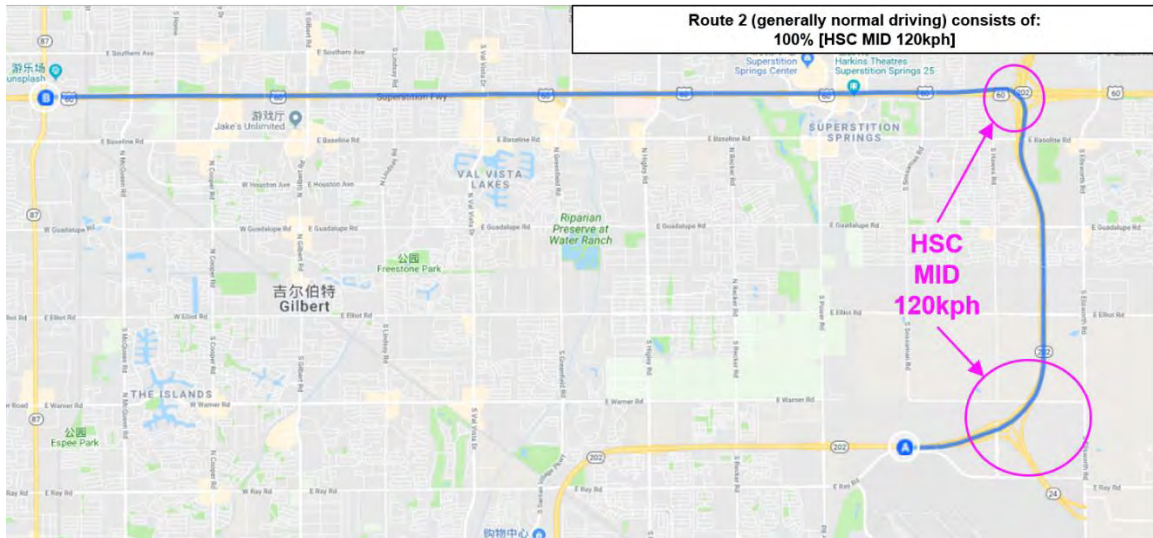


Figure 27. Planning of Route 2 by using Google Maps.

Contrary to the case where aggressive driving strategy is applied, another route is selected to evaluate the rollover probability and consequent loss when the autonomous vehicle is traveling with less aggressive/normal driving strategy. Similarly, the route is planned in Google Maps, and as shown in Figure 27.

In this case, no critical situations are assigned along the planned route, except for two inherent cornering scenarios. Thus, the autonomous vehicle is only required to track the planned route, with speed being roughly set as 120km/h.

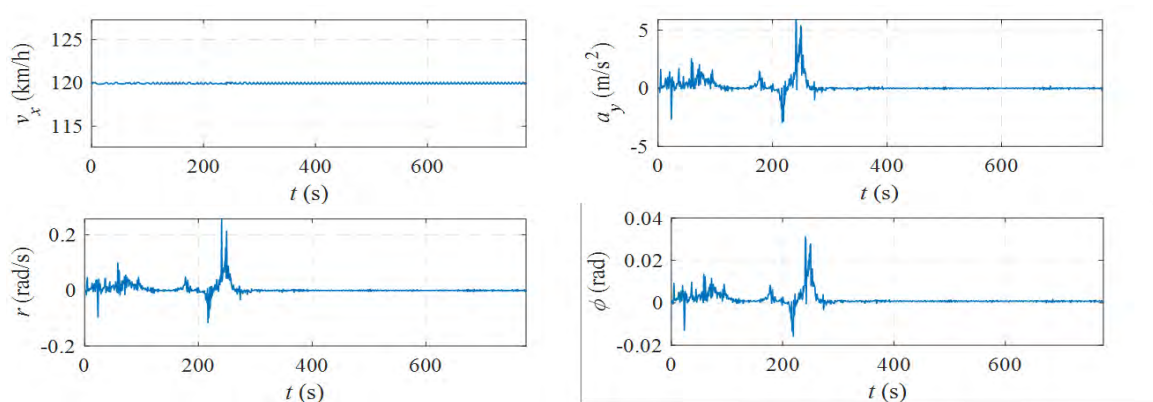


Figure 28. Simulated vehicle dynamics responses for Route 2.

Simulation is conducted to predict the vehicle dynamics responses in the environment of CarSim-Matlab/Simulink. The simulated vehicle dynamics responses are as shown in Figure 28. In comparison with Figure 21, generally much smaller magnitude of a_y , r and ϕ can be observed. The only spot of oscillation in Figure 28 is corresponding to a high-speed cornering maneuver when the vehicle switches from highway 202 to highway 60. This is due to the roughly designed speed profile, which turns out to be unrealistic for an autonomous vehicle to pass this specific part of the route. By using such a speed profile, the vehicle may react aggressively in this cornering maneuver.

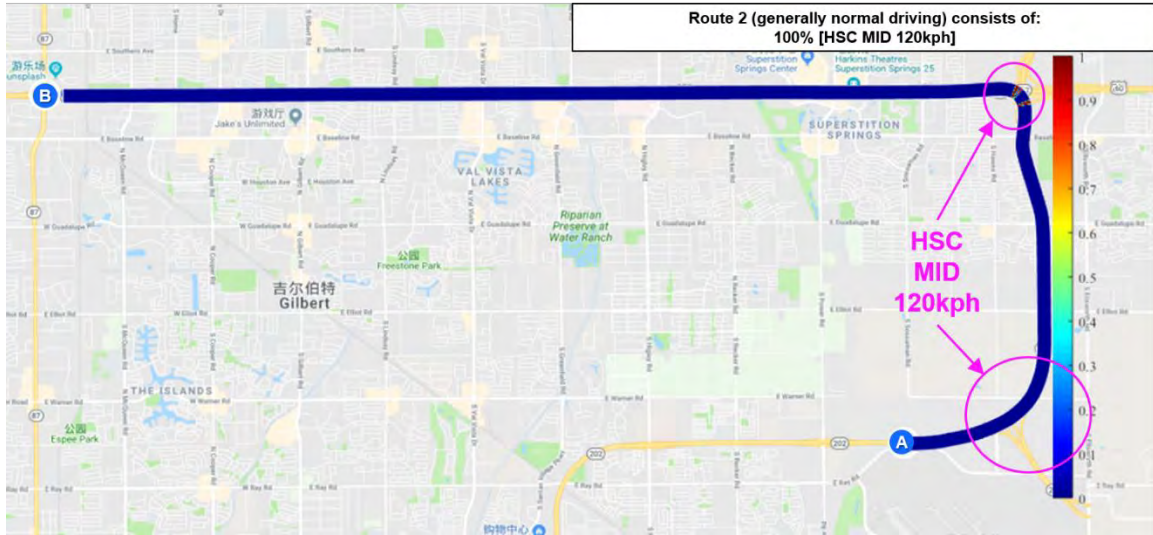


Figure 29. Simulation result of calculated rollover probability along the Route 2.

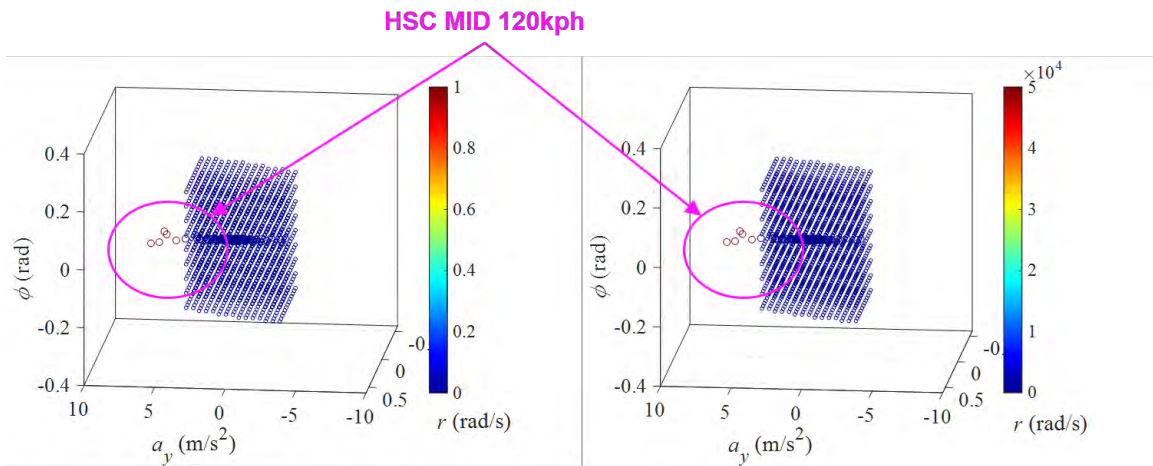


Figure 30. Simulation result of calculated rollover probability (left) and expected loss (right) in state space for Route 2.

Based on the predicted vehicle dynamics responses, our developed methodology is applied for rollover probability evaluation. The resulting rollover probability along the route is, as shown in Figure 29. And the rollover probability and expected loss with respect to the vehicle state trajectory in the 3-D state space (a_y, r, ϕ) are as shown in Figure 30.

As depicted in Figure 29, the overall route possesses a very low rollover probability for an autonomous vehicle, except for the aforementioned high-speed cornering maneuver. The result is consistent with the vehicle dynamics responses in Figure 28.

In addition, compared to Figure 23, a much larger safe/rollover-free region (in blue) can be observed in Figure 30, with most of the vehicle states staying within these safe boundaries. The result indicates that it is very unlikely for autonomous vehicles to suffer from rollover accidents to travel along this route with no critical situations.

Section 5: Simulation and Experimental Validation

To validate the simulation results and compare and contrast them with real-world results, we will use an experimental vehicle in possession of Dr. Chen's lab at Arizona State University.

5.1 The Lab's Vehicle Parameters

The lab has in its possession the Autonomous Ground Vehicle prototype shown in Figure 31. The prototype is equipped with multiple electric motors, thus possesses over-actuation features. The four in-wheel motors can be independently actuated for both tracing and regenerative braking control. Also, the automated steering control is realized via the electric motor in Electronic Powered Steering (EPS) system.

For sensing environmental information, the prototype adopts a look-forward camera for lane detection, a radar for monitoring preceding subjects, and multiple ultra-sonic sensors for sensing surrounding subjective. The vehicle location and states of motion are measured by a high-end IMU/GPS navigator in real-time.



Figure 31. 4IWM AGV prototype and vehicle parameters.

The parameters of the 4-in-wheel-motor autonomous ground vehicle (4-IWM AGV) are $m = 732.5\text{kg}$, $l_f = 1.12\text{m}$, $l_r = 0.96\text{m}$, $L = l_f + l_r$, $w = 1.26\text{m}$ and $h_{cg} = 0.65\text{m}$. Here, m is the vehicle mass, l_f and l_r the distances from center of gravity (CG) to front and rear axles, respectively, L the wheel base, w the track width, and h_{cg} the CG height.

5.2 Validation Process

An example of both simulation and experimental validation is given as below:

- (1) A route from point A to point B was firstly planned by using Google Maps, as shown in Figure 32.

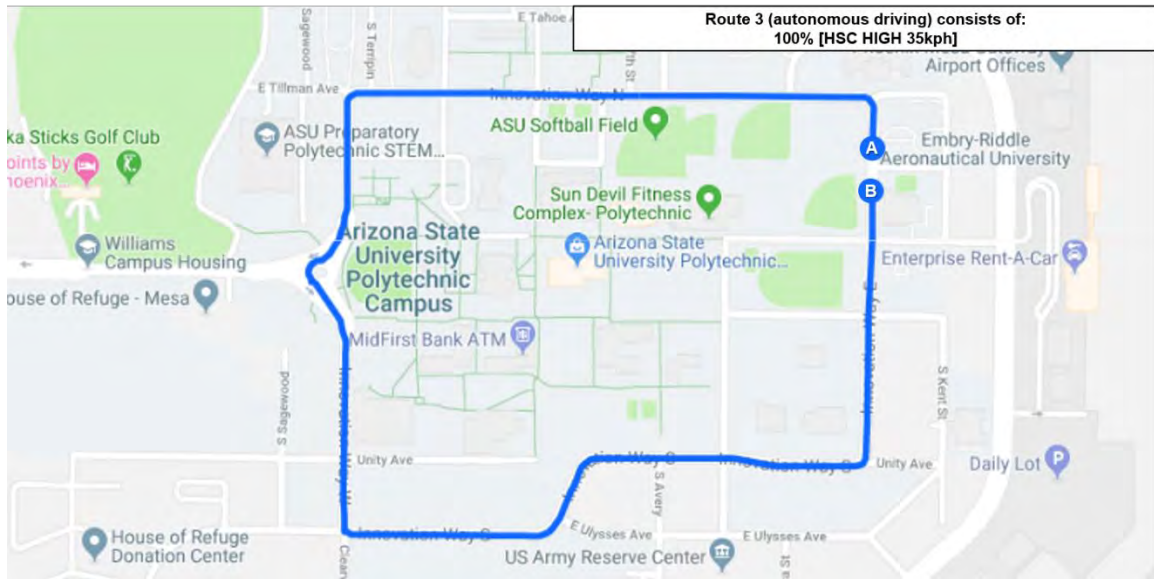


Figure 32. A route around the Polytechnic Campus of Arizona State University.

- (2) For experiments, a field test using the 4-in-wheel-motor (4-IWM) autonomous ground vehicle (AGV) prototype was carried out by the Dynamic Systems and Control Laboratory (DSCL). In the experiment the 4-IWM AGV prototype was fully driven by a developed autonomous driving system to track the desired route generated in (1). The 4IWM AGV prototype is as shown in Figure 31;
- (3) For simulations, the route coordinates are extracted from the *.kml file exported from Google Maps, and imported to CarSim to generate geometric path. The experimental data of vehicle velocity profile is used as the target speed for tracking;
- (4) The co-simulation is conducted in CarSim-Matlab/Simulink environment;
- (5) The simulation results in comparison with the experimental results are as shown in Figure 33. The results show that the simulation matches well with the experiment, suggesting the adopted simulation methods and settings can realistically reflect the actual vehicle dynamics responses, thus can be used for predicting vehicle states in other cases;

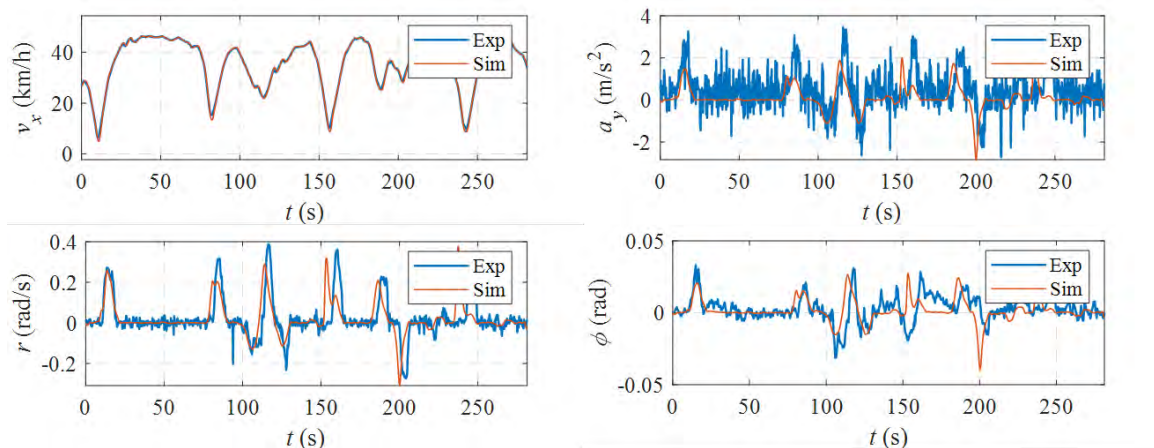


Figure 33. Comparison of simulation and experimental results of vehicle dynamics responses.

- (6) Both simulation and experimental data, respectively, are used in calculating the rollover probability along the planned trajectory, coupled with the rollover probability and the estimated loss with respect to the vehicle state trajectory in the 3-D state space (a_y, r, ϕ) , etc. The results are as shown from Figure 34 to Figure 37, respectively. As usual, with bold dots, the trajectory vehicle travels in state space, is embedded in the rollover region.

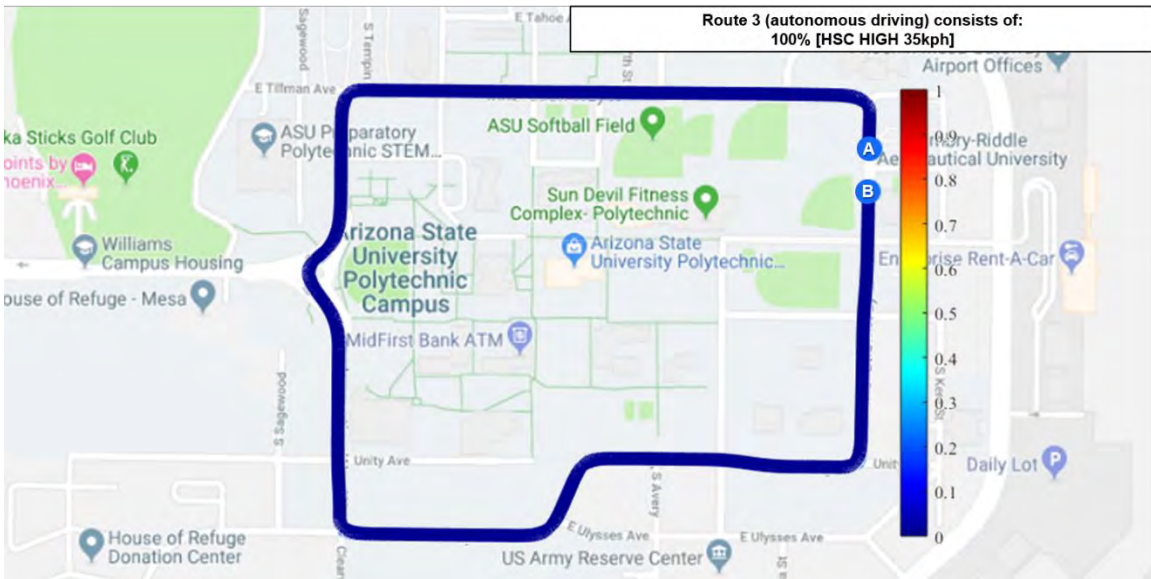


Figure 34. Simulation result of calculated rollover probability along the planned trajectory.

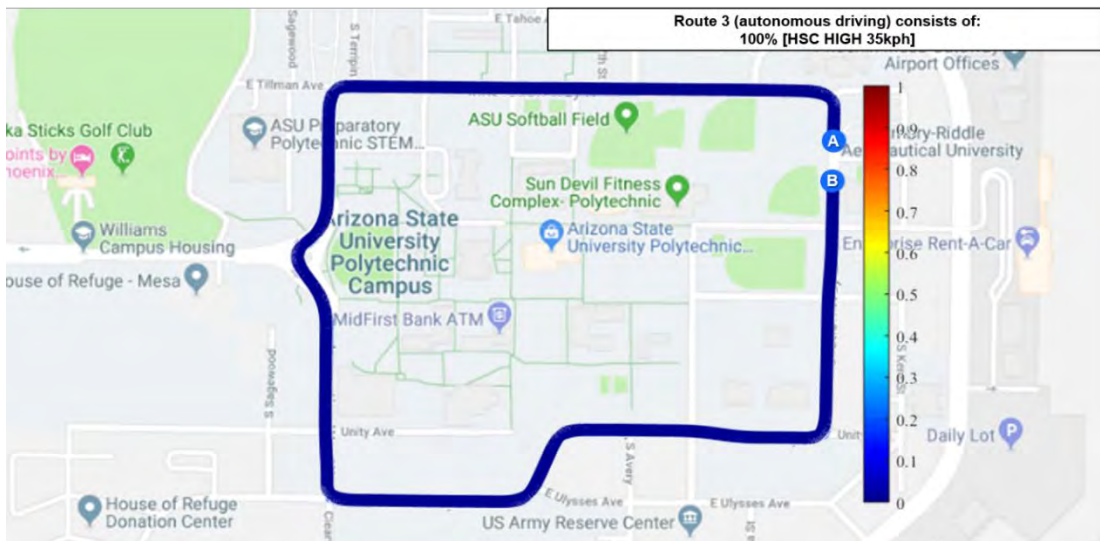


Figure 35. Experimental result of calculated rollover probability along the planned trajectory.

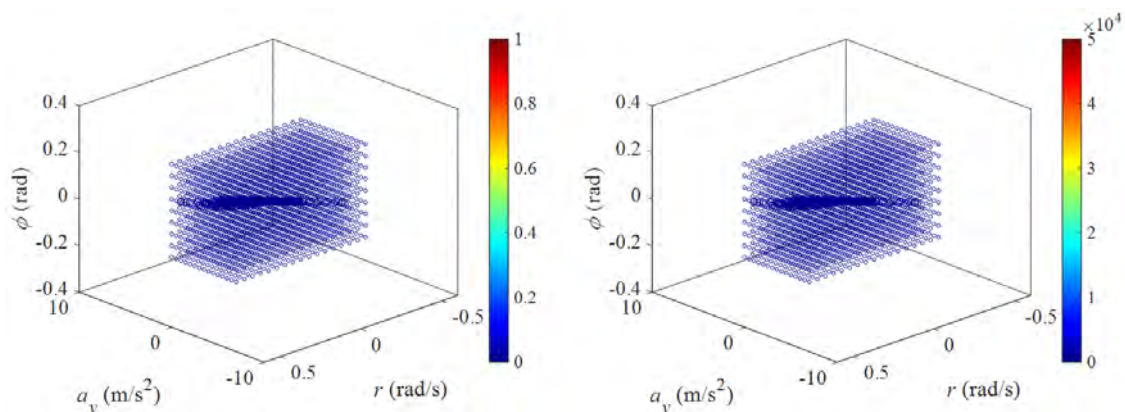


Figure 36. Simulation result of calculated rollover probability and estimated loss in 3-D state space (a_y, r, ϕ) .

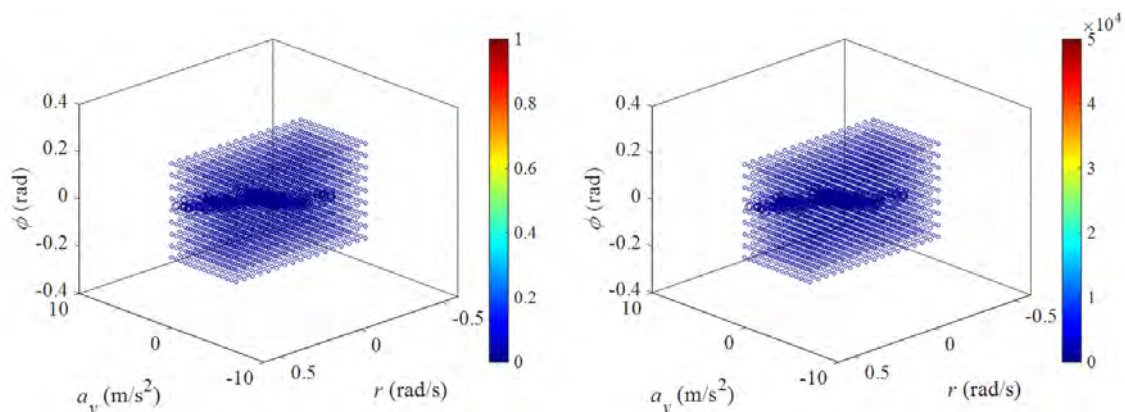


Figure 37. Experimental result of calculated rollover probability and estimated loss in 3-D state space (a_y, r, ϕ) .

As expected, given the maximum speeds kept in the experimental setting, the probabilities of rollover are insignificant. Due to the potential risk of the experimental vehicle, the experiments involving higher speeds were not attempted.

Appendix A: QQ Plots

The QQ plots below present serve the purpose of illustrating how observed distributions in state space dimensions of a_y , r , ϕ compare to normal distribution. The x-axis presents quantiles of normal distribution while y-axis an empirical distribution of a given state space dimension.

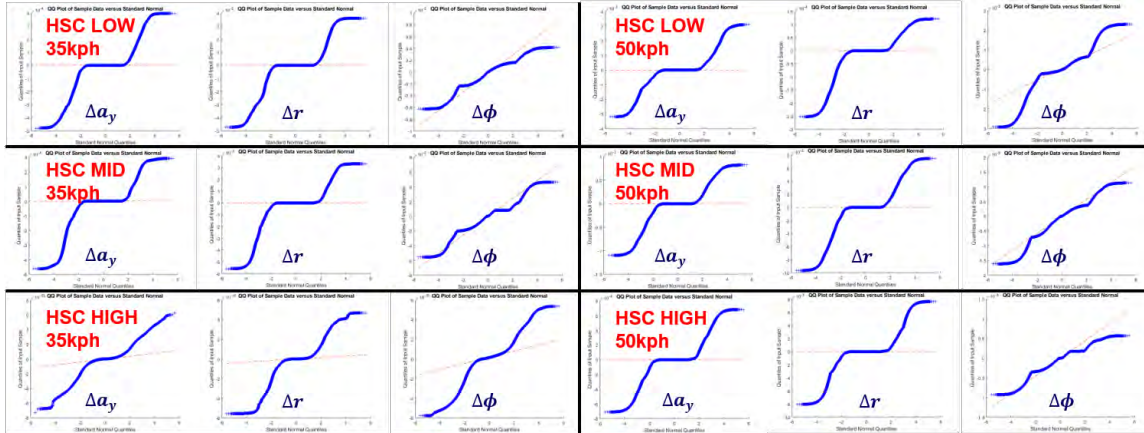


Figure 208. QQ plots for HSC offset given LOW, MID and HIGH road quality (35 kph and 50 kph)

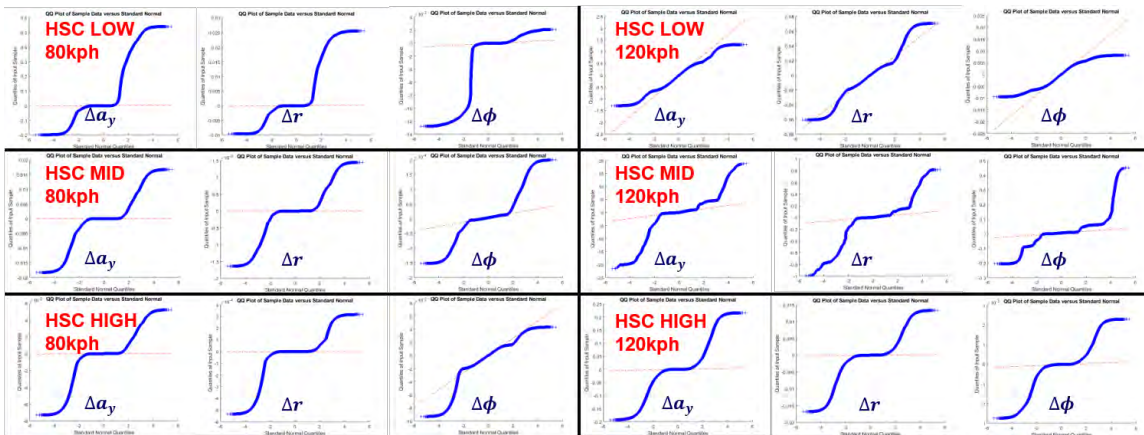


Figure 39. QQ plots for HSC offset given LOW, MID and HIGH road quality (80 kph and 120 kph)

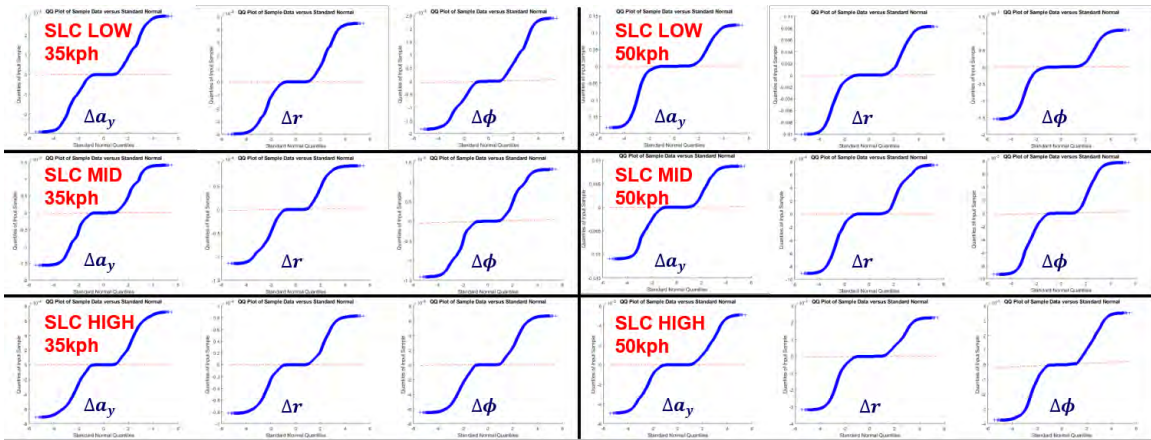


Figure 40. QQ plots for SLC offset given LOW, MID and HIGH road quality (35 kph and 50 kph)

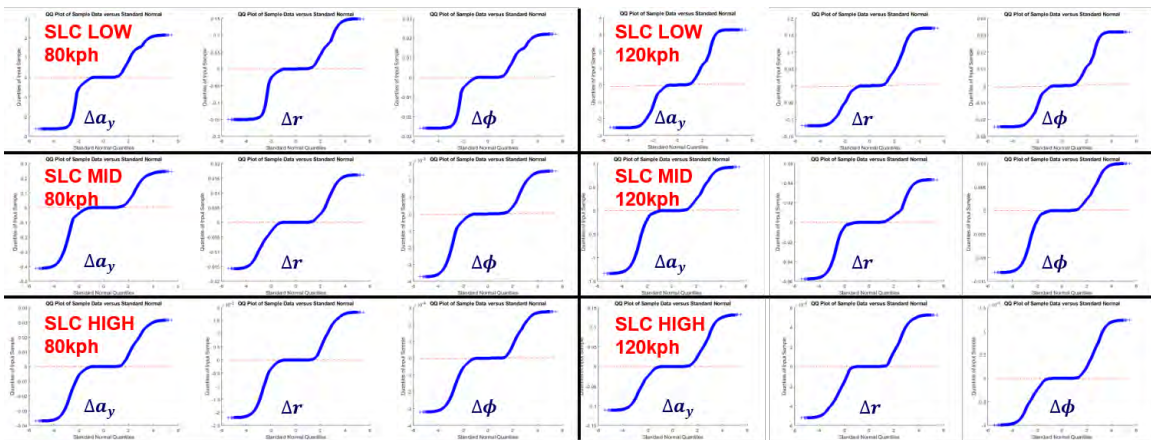


Figure 41. QQ plots for SLC offset given LOW, MID and HIGH road quality (80 kph and 120 kph)

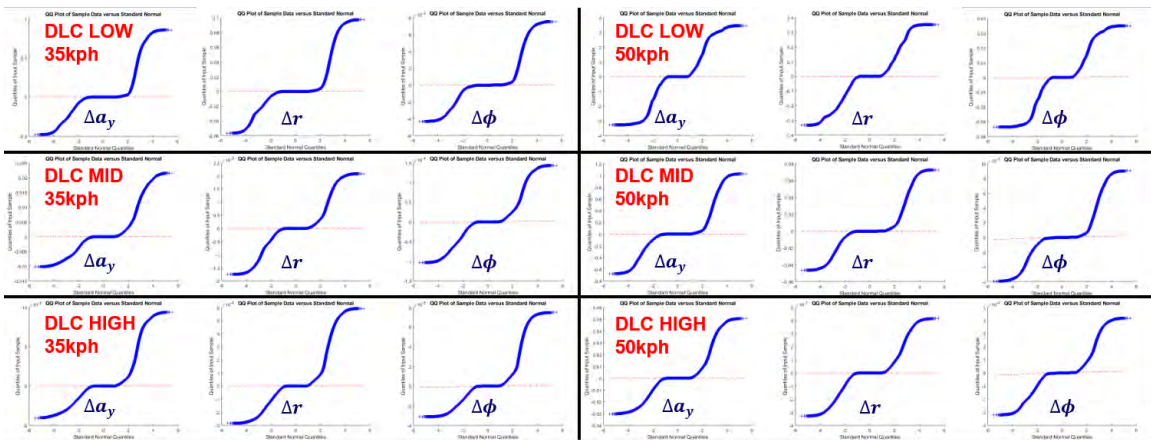


Figure 42. QQ plots for DLC offset given LOW, MID and HIGH road quality (35 kph and 50 kph)

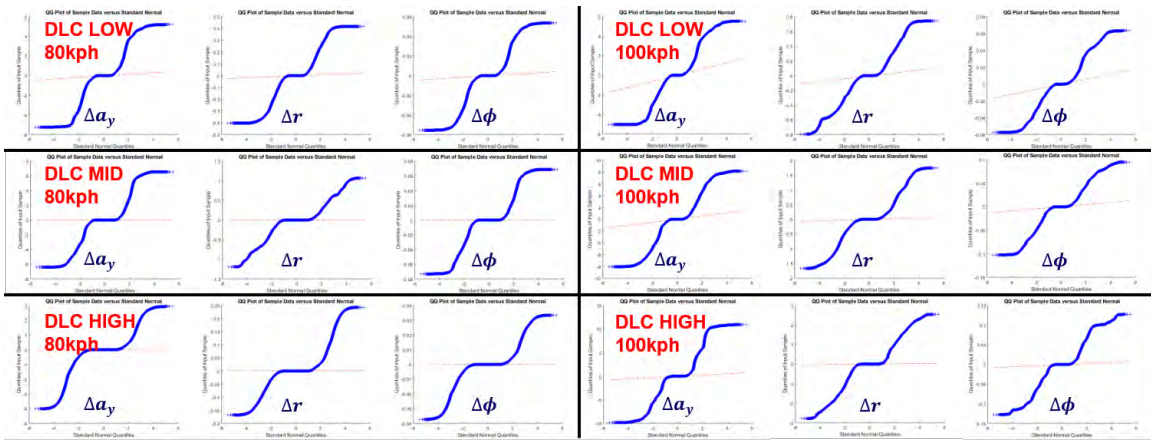


Figure 43. QQ plots for HSC offset given LOW, MID and HIGH road quality (80 kph and 100 kph)

Endnotes

Rollover is one of the most critical safety issues for vehicles, specifically those with higher center of gravity (CG) such as sport utility vehicles (SUVs), pickup vans and trucks. According to the 2009 annual report from the National Highway Traffic Safety Administration (NHTSA), up to 8732 vehicles were involved in fatal crashes due to rollover. The statistics of rollover accidents showed that 54.4% of vehicle occupant fatalities in single-vehicle crashes involved a rollover event. In 2010, though only contributed to 2.1% of 9.1 million total crashes of passenger cars, SUVs and pickup vans, rollovers accounted for approximately 35% of all deaths from these accidents, with more than 7600 people losing their lives.

One of the promises of autonomous vehicles is comprehensively addressing vehicle safety issues, including rollover. This is envisioned to be achieved by eliminating human errors and restricting vehicle behaviors within safe/stable dynamical regions. It is only by developing and implementing high-end automated safety control systems based on comprehensive understanding of vehicle dynamics, a large percent of the risks can be mitigated or prevented on the spot in real-time. With the developed probabilistic model of rollover risk that thoughtfully describes the vehicle rollover behaviors, this research advances these solutions one big step further.

In conclusion, in this research, we develop an effective theoretical, high-fidelity simulation verified, and preliminary experiments validated rollover risk prediction/evaluation methodology, which is applicable in the phase of trajectory planning. A safer performance of autonomous vehicles is believed to be achieved with the advent of this methodology in applications. For example, trajectories with higher risk can be avoided in the phase of planning, or the autonomous driving systems can get 'prepared' before the incoming critical situations. Therefore, technologies as this may have a profound impact on the development of autonomous vehicles, as vehicle safety can be better ensured, and lives can be saved. Also, with this research, the insurer not only possesses the necessary tools to access the riskiness of the new autonomous driving system when it comes to rollover risk but also can, in practice, promote meaningful safety change and help save lives. Finally, from the methodological point of view, the broader implication of this research is establishing a conceptual framework to characterize (other) vehicle dynamics risks of autonomous vehicles probabilistically. This constitutes a novel direction of research in automobile safety and paves the way for insurers to understand a large part of the multifaced risk that autonomous vehicles bring.

As their commercial exploitation in the immediate future will be most economically impactful, further research involves applying the developed framework to autonomous trucks (and autonomous trucks with trailers) as the complexity of their physics will require additional methodological considerations. When it comes to autonomous vehicles' dynamics, the next risk to be investigated is understeering and oversteering risk. Additionally, modeling the human driver and investigating semi-autonomous driving settings from a risk perspective is a promising research direction. Finally, understanding and articulating implications of this work for the purpose of insurance and safety legislation of autonomous vehicles is an important research direction made available by contributions of this research.

References

- [1] Anderson, J. M., Nidhi, K., Stanley, K. D., Sorensen, P., Samaras, C., & Oluwatola, O. A. (2014). Autonomous vehicle technology: A guide for policymakers. Rand Corporation.
- [2] Falcone, P., Borrelli, F., Asgari, J., Tseng, H. E., & Hrovat, D. (2007). Predictive active steering control for autonomous vehicle systems. *IEEE Transactions on control systems technology*, 15(3), 566-580.
- [3] Kritayakirana, K., & Gerdes, J. C. (2012). Autonomous vehicle control at the limits of handling. *International Journal of Vehicle Autonomous Systems*, 10(4), 271-296.
- [4] Brown, M., Funke, J., Erlien, S., & Gerdes, J. C. (2017). Safe driving envelopes for path tracking in autonomous vehicles. *Control Engineering Practice*, 61, 307-316.
- [5] González, D., Pérez, J., Milanés, V., & Nashashibi, F. (2015). A review of motion planning techniques for automated vehicles. *IEEE Transactions on Intelligent Transportation Systems*, 17(4), 1135-1145.
- [6] Phanomchoeng, G., & Rajamani, R. (2012). Prediction and Prevention of Tripped Rollovers. Department of Mechanical Engineering, University of Minnesota.
- [7] Dobbins, H. L. (1989). U.S. Patent No. 4,847,589. Washington, DC: U.S. Patent and Trademark Office.
- [8] Chen, B. C., & Peng, H. (2001). Differential-braking-based rollover prevention for sport utility vehicles with human-in-the-loop evaluations. *Vehicle System Dynamics*, 36(4-5), 359-389.
- [9] Carlson, C. R., & Gerdes, J. C. (2003, November). Optimal rollover prevention with steer by wire and differential braking. In *Proceedings of IMECE* (Vol. 3, pp. 16-21).
- [10] Lu, J. (2010). U.S. Patent No. 7,647,148. Washington, DC: U.S. Patent and Trademark Office.
- [11] Woodrooffe, J. H. F. (1993, April). Practical concepts in heavy truck rollover accident analysis. In *Heavy Vehicle Rollovers Conference* (pp. 29-30).
- [12] Rakheja, S., & Piche, A. (1990). Development of directional stability criteria for an early warning safety device. *SAE transactions*, 877-889.
- [13] Preston-Thomas, J., & Woodrooffe, J. H. (1990). Feasibility Study of a Rollover Warning Device for Heavy Trucks.
- [14] Freedman, M., Olson, P. L., & Zador, P. L. (1992). Speed actuated rollover advisory signs for trucks on highway exit ramps.
- [15] McGee, H., Joshua, S., Hughes, W., Strickland, R., & Bareket, Z. (1993). Feasibility of An Automatic Truck Warning System (No. FHWA-RD-93-039).
- [16] Bouteldja, M. (2005). Modélisation des Interactions dynamiques poids lourds/infrastructures pour la sécurité et les alertes (Doctoral dissertation, Versailles-St Quentin en Yvelines).
- [17] Imine, H., & Dolcemascolo, V. (2007). Rollover risk prediction of heavy vehicle in interaction with infrastructure. *International Journal of Heavy Vehicle Systems*, 14(3), 294-307.
- [18] Rajamani, R. (2011). *Vehicle dynamics and control*. Springer Science & Business Media.
- [19] Larish, C., Piyabongkarn, D., Tsourapas, V., & Rajamani, R. (2013). A new predictive lateral load transfer ratio for rollover prevention systems. *IEEE Transactions on Vehicular Technology*, 62(7), 2928-2936.
- [20] Phanomchoeng, G., & Rajamani, R. (2012). New rollover index for the detection of tripped and untripped rollovers. *IEEE Transactions on Industrial Electronics*, 60(10), 4726-4736.
- [21] Chen, B. C., & Peng, H. (1999, June). A real-time rollover threat index for sports utility vehicles. In *Proceedings of the 1999 American Control Conference* (Cat. No. 99CH36251)(Vol. 2, pp. 1233-1237). IEEE.
- [22] Chen, B., & Peng, H. (1999, November). Rollover warning of articulated vehicles based on a time-to-rollover metric. In *ASME International Mechanical Engineering Conference and Exhibition*.
- [23] Choi, S. B. (2008). Practical vehicle rollover avoidance control using energy method. *Vehicle System Dynamics*, 46(4), 323-337.
- [24] Wang, F., & Chen, Y. (2017, October). Detection of vehicle tripped and untripped rollovers by a novel index with mass-center-position estimations. In *ASME 2017 Dynamic Systems and Control Conference* (pp. V003T33A003-V003T33A003). American Society of Mechanical Engineers.
- [25] Wang, F., & Chen, Y. (2019). Vehicle rollover propensity detection based on a mass-center-position metric: a continuous and completed method. *IEEE Transactions on Vehicular Technology*, Vol. 68, No. 9, pp. 8652-8662, 2019.

- [26] Yakub, F., & Mori, Y. (2015). Enhancing path following control performance of autonomous ground vehicle through coordinated approach under disturbance effect. *IEEJ Transactions on Electronics, Information and Systems*, 135(1), 102-110.
- [27] Yakub, F., Abu, A., Sarip, S., & Mori, Y. (2016). Study of model predictive control for path-following autonomous ground vehicle control under crosswind effect. *Journal of Control Science and Engineering*, 2016.
- [28] Hu, J. S., Wang, Y., Fujimoto, H., & Hori, Y. (2017). Robust yaw stability control for in-wheel motor electric vehicles. *IEEE/ASME Transactions on Mechatronics*, 22(3), 1360-1370.
- [29] Rajamani, R., Piyabongkarn, N., Lew, J., Yi, K., & Phanomchoeng, G. (2010). Tire-road friction-coefficient estimation. *IEEE Control Systems Magazine*, 30(4), 54-69.
- [30] Khaleghian, S., Emami, A., & Taheri, S. (2017). A technical survey on tire-road friction estimation. *Friction*, 5(2), 123-146.

About The Society of Actuaries

The Society of Actuaries (SOA), formed in 1949, is one of the largest actuarial professional organizations in the world dedicated to serving more than 32,000 actuarial members and the public in the United States, Canada and worldwide. In line with the SOA Vision Statement, actuaries act as business leaders who develop and use mathematical models to measure and manage risk in support of financial security for individuals, organizations and the public.

The SOA supports actuaries and advances knowledge through research and education. As part of its work, the SOA seeks to inform public policy development and public understanding through research. The SOA aspires to be a trusted source of objective, data-driven research and analysis with an actuarial perspective for its members, industry, policymakers and the public. This distinct perspective comes from the SOA as an association of actuaries, who have a rigorous formal education and direct experience as practitioners as they perform applied research. The SOA also welcomes the opportunity to partner with other organizations in our work where appropriate.

The SOA has a history of working with public policymakers and regulators in developing historical experience studies and projection techniques as well as individual reports on health care, retirement and other topics. The SOA's research is intended to aid the work of policymakers and regulators and follow certain core principles:

Objectivity: The SOA's research informs and provides analysis that can be relied upon by other individuals or organizations involved in public policy discussions. The SOA does not take advocacy positions or lobby specific policy proposals.

Quality: The SOA aspires to the highest ethical and quality standards in all of its research and analysis. Our research process is overseen by experienced actuaries and nonactuaries from a range of industry sectors and organizations. A rigorous peer-review process ensures the quality and integrity of our work.

Relevance: The SOA provides timely research on public policy issues. Our research advances actuarial knowledge while providing critical insights on key policy issues, and thereby provides value to stakeholders and decision makers.

Quantification: The SOA leverages the diverse skill sets of actuaries to provide research and findings that are driven by the best available data and methods. Actuaries use detailed modeling to analyze financial risk and provide distinct insight and quantification. Further, actuarial standards require transparency and the disclosure of the assumptions and analytic approach underlying the work.

Society of Actuaries
475 N. Martingale Road, Suite 600
Schaumburg, Illinois 60173
www.SOA.org